DEMOCRATIC AND POPULAR ALGERIAN REPUBLIC MINISTRY OF HIGHER EDUCATION AND SCIENTIFIC RESEARCH

MOHAMED KHIDER UNIVERSITY OF BISKRA

FACULTY OF SCIENCE AND TECHNOLOGY
DEPARTMENT OF ELECTRICAL ENGINEERING

Doctorat thesis in Sciences
Specialty: Electronic

Presented by:
Rouis Mohamed

Title of these ::

The analysis of the pathological linear association degree of a phonocardiogram (PCG) signals by applying coherences

The members of jury :

Pr. Salim SBAA	University of Biskra	President
Pr. Abdelkrim OUAFI	University of Biskra	Rapporteur
Pr. Abdelmalik TALEBAHMED	University of Valenciennes, France	Examiner
Pr. Mahmoud TAIBI	University of Annaba	Examiner
Dr. Athmane ZITOUNI	University of Biskra	Examiner
Dr. Riadh AJGOU	University of Eloued	Examiner

2018/2019

Abstract

   The recorded phonocardiogram PCG signal is often contaminated by different types of noises that can be seen in the frequency band of PCG signal, which may change the characteristics of this signal. Discrete wavelet transform (DWT) has become one of the most important and powerful tools of signal representation, but its effectiveness is influenced by the issue of the selected mother wavelet and decomposition level (DL). The selection of DL and the mother wavelet are the main challenges. This work proposes a new approach for finding an optimal DL and optimal mother wavelet for PCG signals denoising. Our approach consists of two algorithms are designed to tackle the problems of noise and variability caused by PCG acquisition in a real clinical environment for different categories of patients whereas the obtained results are evaluated by examining coherence analysis, correlation coefficient, and in term of mean square error (MSE) and signal-to-noise ratio (SNR) in simulated noisy PCG signals. The experimental results show that the proposed method can effectively reduce noise.

Keywords: denoising operation, mother wavelet selection, optimal decomposition level, PCG signal

Résumé

Le signal phonocardiogramme PCG représente l'enregistrement sonore des bruits cardiaques, il peut contenir plusieurs types de bruit qui peut être observé dans la bande de fréquence de signal que permet modifier les caractéristiques de ce dernier. La transformée discrète en ondelettes (TDO) est devenue l'un des outils les plus importants et les plus puissants de la représentation des signaux, mais son efficacité est influencée par la sélection du niveau de décomposition et de l'ordre de l'ondelette, ce sont les principaux défis. Notre travail propose une nouvelle approche pour trouver le niveau et l'ordre optimaux pour le débruitage des signaux PCG. Cette approche est composée de deux algorithmes pour aborder les problèmes de bruit et de variabilité causés par l'acquisition de PCG dans un environnement clinique réel pour différentes catégories de patients . les résultats obtenus sont évalués en examinant l'analyse de cohérence, le coefficient de corrélation et l'erreur quadratique moyenne (MSE) et le "rapport signal/bruit" (SNR). Les résultats montrent que notre méthode effectivement réduire le bruit.

Mots clés: opération de débruitage, sélection de l'ondelette mère, niveau de décomposition optimal, signal PCG

ملخــــص الاطـــروحـــــة

كثيـراً مـا يكـون مخطـط أصـوات القلـب PCG مصحوباً بأنـواع مختلفـة مـن الضوضـاء التي يمكـن رؤيتهـا في نطـاق تـردد إشـارة PCG ، والتي قـد تغيـر خصـائص هـذه الإشـارة. أصبـح تحويـل المويجـات المتقطـعة (DWT) أحـد أهـم وأقـوى أدوات معالجـة الإشـارات ، ولكـن فعاليتهـا تتأثـر بمسـألة مسـتوى التحليـل (DL). إن اختيـار DL والموجـة الأم هـي التحديـات الرئيسيـة في الوقـت الحالـى.

في هذه الاطروحـة نقتـرح أسلوبًـا جديـدًا لإيجـاد مسـتوى التحليـل وموجـة الأم المثلـى. في هذا النطـاق، عملنـا يتكـون مـن اثنيـن مـن الخوارزميـات مصممـة في عمليـة لإزالـة الضجيـج الموجـود في اشـارة PCG في بيئـة سريريـة حقيقيـة للحـالات المرضيـة، في حيـن يتـم تقييـم النتائـج التي تم الحصـول عليهـا مـن خـلال دراسـة تحليـل الاتسـاق (Coh) ومعامـل الترابط (corr.coef)، مـع الخطـأ التربيعـي المتوسط (MSE) و نسبـة الإشـارة إلى الضجيـج (SNR). تظهـر النتائـج التجريبيـة أن الطريقـة المقتـرحـة يمكـن أن تقلـل الضوضـاء بشكـل فعـال.

الكلمــات الرئيسيـــــة: عمليـة تقليـل الضوضـاء ، حجـز موجـة الأم المثلـى ، حجـز مستـوى التحليـل الأمثـل ، إشـارة PCG

Table of Contents

Chapter 2
Wavelet Transforms for signals

Chapter 3
The Usefulness of Wavelet Transform to Reduce Noise in the PCG Signal

Chapter 4
Experimental Results and Performance Evaluation

List of Figures

List of Table

List of symbols and abbreviations	
EC2	ejection click
SG	diastolic summation Gallop
SW	diastolic wide S2 split
SAS	severe systolic-aortic stenosis
PS	Systolic Pulmonary Stenosis
SAS	Severe Systolic Aortic Stenosis
SG2	Diastolic Summation Gallop II
SNRs	The signal to noise ratio related to symelet wavelet
SNRd	The signal to noise ratio related to Daubechie wavelet
Ks	coefficient distortion
PCG	phonocardiogram
coh	Coherence
Corr	Correlation coefficient
DL	decomposition levels
DO	Orders
MSE	mean square error
FIR	Finite impulse response
DWT	Discrete wavelet transform
IDWT	Inverse discrete wavelet transform
CWT	Continuous wavelet transform
FWT	Fast wavelet transform
cov	covariance
MRA	Multi-Resolution Analysis
$\{V_j\}_{j \in Z}$	approximation spaces
STFT	short time fourier transform
H	low-pass filter
G	high-pass filter
ϕ	scaling function
ψ	mother wavelet
WS	wavelet series
τ	Location parameter
s	scale parameter
σ	deviation of noise
AWGN	Additive White Gaussian noise

General Introduction

General Introduction

Phonocardiography (PCG) deals with processing of the acoustic signals produced by the mechanical actions of the heart resulting in the vibration of the valves, heart muscle tissues and great vessels. One of the central issues is to extract the different heart sounds from a noisy recording and relate them to the corresponding cardiac event. Moreover, heart sounds can be further analysed and certain features can be extracted for estimating the underlying cardiac parameters.

The importance of the heart was already realized in the fourth century B.C., although with some misconceptions: Aristotle argued that it was the seat of intelligence, motion and sensation. From the medical perspective, Hippocrates noted already an early form of auscultation by holding an ear against the chest, but in his works he described only breathing sounds. Blood circulation was first described by William Harvey, an English Physician in 1628. Nowadays, because of new advances in cardiac imaging, cardiac auscultation has become a preliminary test in the primary health care. On the other hand, due to the limited financial and human expert resources and the development of modern low cost computational devices in information technology, phonocardiography emerges also as a topic of current research and a possible tool aiding clinical decision making. One of the greatest problems in recording heart sound is noise parasitic effects.

A reasonable solution to noise reduction can be carried out in two parts. First, extraneous noises must be minimized in the vicinity of the patient during recording. Second, signal processing methods must be effective in noisy environments. The PCG signal discloses information about cardiac function through vibrations caused by the working heart. The heart sound signals are very weak in range, from 10 Hz to 250 Hz, and they can be easily subject to interference from various noise sources [1]. These various noise components make the diagnostic evaluation of PCG records difficult or even impossible in some cases. Observed signals as PCGs in nature usually show non-stationary and multi-temporal scale characteristics.

The separation of noise from PCG recordings proves a more problematic task due to their inherent overlap in frequency and temporal domains. De-noising methods used presently are mainly based on simulation model or spectral analysis [2], and they cannot reveal these complicated characteristics of signals and thus cannot satisfactorily meet practical needs. In the other hand, Denoising is a substantial issue in signal analysis because noise has a great influence on the real characteristics of the signal [3]. The denoising techniques used to remove the additive noise while retaining as much as possible the important signal features, such as the technique of Independent Component Analysis, Principle Component

Analysis [4]. Compared with them, the discrete wavelet transform (DWT) method is more effective and is especially applicable in various engineering applications such as medicine, physics,.. etc., because it can elucidate the localized characteristics of non-stationary signals both in the temporal and frequency domains [5]. Hence, DWT has been widely adopted in biomedical signal processing, because it has the ability to capture the energy of signals in few energy and it can be separate noise from signal. However, in the current study only orthogonal wavelets are examined since they allow perfect reconstruction of a signal. While many key issues impact the DWT and the most logical question at this point is how to choose a mother wavelet and decomposition level, although many studies have been conducted presently. These issues have not been completely solved. Selecting decomposition levels and mother wavelet to denoise signal are a major challenge to which current methods do not provide guidance.

Framework of the thesis

This the work focus on selecting the optimal DL and the best mother wavelet for PCG signal, which are more appropriate for real time denoising operation. The results of study will be between Symlet and Daubechies wavelet family under simulative noise added to the clean signal.This thesis is structured in four main chapters.

Chapter (1) presents a literature review covering the basic principles of the cardiovascular system, how the different heart sounds are produced and gives an introduction to auscultation and phonocardiography. Chapter (2) presents an introduction to Wavelets. Chapter (3) explains the procedure of the signal denoising using wavelet transform through thresholding fuctions and threshold estimation with the proposed method. In this thesis, Experimental results and discussion are presented in chapter (4). Finally, presents the conclusions

ii

Chapter 1

The physiological origin of the heart sound and the murmurs

1.1 Introduction

Heart sounds are generated by the interactions between heart chambers, valves and great vessels and the blood flowing through them. Mechanical vibrations reflect the turbulence that occurs when heart valves close. Traditionally, a stethoscope is used in cardiac auscultation to listen to these sounds that provide important acoustic information regarding the condition of the heart. The transient nature of the PCG signal deprived it from pioneering medical signals aimed for cardiac exploration. Moreover, the controversy still blurring the origin of heart sounds and murmurs. Indeed, heart sounds and murmurs, going across the tissues between the heart and the thorax, are transmuted by the filtering effect of the heart–thorax system [6, 7]. Furthermore, recording heart sounds and murmurs from various thoracic sites complicates the analysis and comparison of the acquired PCG signals. When computers's dawn broke, a new era loomed up yielding digital phonocardiography. Hence, data acquisition gave a new perception of heart sounds and murmurs as digital phonocardiogram signal which can be stored within a computer. Moreover, the advents of digital signal processing techniques enable digital phonocardiography to benefit from new processing methods. Resonant features of heart valves as well as blood flow turbulence within heart cavities can be digitally quantified. Therefore, digital phonocardiography became a reliable tool for detecting valvular pathologies as well as preventing valvular prosthesis dysfunction. Thus, several researchers watched over analysis of heart sounds and murmurs by advanced digital signal processing methods. Hence, the PCG signal can provide a valuable medical diagnosis towards exploration of the cardiac activity. This chapter starts with a brief description of the anatomy of the heart that is complemented with a brief introduction on the origin of heart sounds. Since heart sounds are originated as a consequence of the vibration of the heart valves and shear stress of the blood on the surface of the heart vessels, it is important to highlight the physical components of the cardiac muscle that are most active.

1.2. Heart's Anatomy and Physiology

The heart is a constituent of the cardiovascular system located in the lower thorax, in the middle mediastinum slightly to the left of the mid sagittal plane and in relation to vessels: the superior and inferior vena cava, the pulmonary artery and vein, and aorta [8]. It weighs about 250 to 300 grams, and its wall is composed of cardiac muscle, also called myocardium; the heart has four compartments/chambers: the right and left atria and right and left ventricles. The heart is oriented such a ways that the anterior aspect is the right ventricle while the posterior Aspects shows the left atrium, see Figure (1.1) the upper atria compartments

are constituted as one unit and the lower ventricles as another. The left ventricular free wall and the septum are much thicker than the right ventricular wall. The function of the heart is to receive oxygenated blood from the lungs and to supply it to every organ of the body. In order to execute its function, the heart has four chambers and four types of valves. During the pumping process, blood is forced through the valves, out of the chambers when the heart contracts, flowing from one chamber to another.
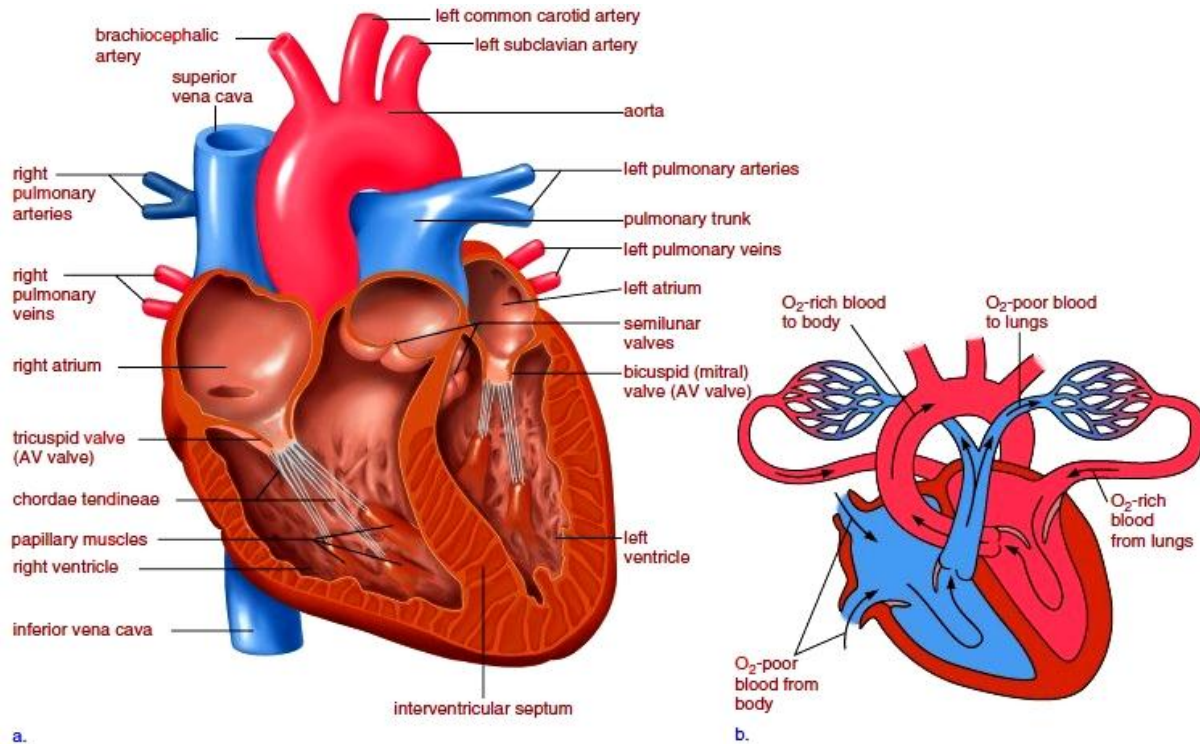
Figure (1.1). *(Left) Anatomy of the heart and physiology (right) blood flow through the chambers of the heart.*

The pumping action of the heart is divided into two phases: systole when the ventricles contract and eject blood from the heart, and diastole, when the ventricles are relaxed and the heart is filled with blood. Four valves prevent the blood from flowing backwards; the atrio-ventricular valves (mitral and tricuspid) prevent blood flowing back from the ventricles to the atria and the semilunar valves (aortic and pulmonary valves) prevent blood from flowing back towards the ventricles once being pumped into the aorta and the pulmonary artery, respectively. Deoxygenated blood of the body enters the right atrium, passes into the right ventricle and is ejected out through the pulmonary artery on its way to the lungs. Oxygenated blood from the lungs re-enters the heart in the left atrium, passes into the left ventricle and is then ejected out to throughout the body.

1.2.1. Heart Valves

Heart valves are passive elements consisting of connective tissue, responsible for the unidirectional blood flow. The atrioventricular valves that is the mitral and tricuspid valves separate the atria and ventricles, whereas the semilunar valves, called the aortic and pulmonary valves are located at the outflow of the ventricles. There is a single fibrous ring around each of the heart valves, and these rings are connected forming a fibrous skeleton. This framework has several physiological functions: it is the base, to which the heart valves and great arteries attach, and it protects the valves from overstretching as the blood passes through them; furthermore, it behaves as an isolating layer between the atria and ventricles preventing them from simultaneous contraction. All four valves consist of so called leaflets or cusps (Fig. 1.2)[9]. Except the mitral valve, all other valves have three cusps. The main difference between the atrioventricular and semilunar valves is that the atrioventricular valves are connected to the ventricular wall via the tendinous chords. These tendons prevent the valves from turning over into the atria when the ventricles contract to push the blood out into the great arteries. There is less danger of prolapse in the case of the semilunar valves since they have to resist much smaller pressure gradients.
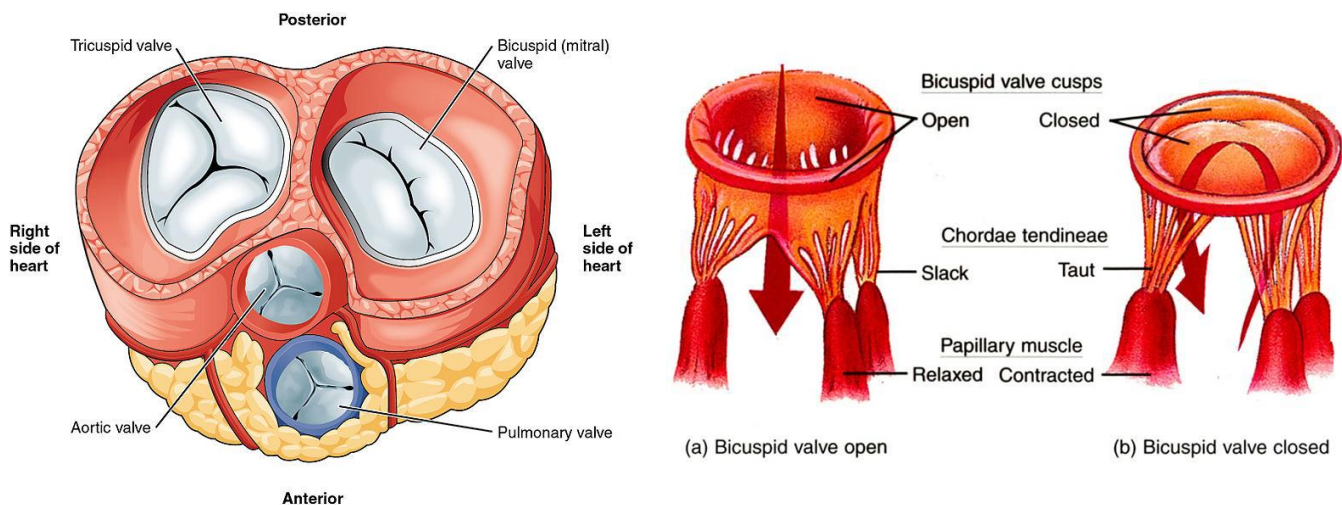
Figure . (1.2). *Heart valves are present at the connections of the atria and ventricles, as well as the pulmonary artery and aorta to achieve a single flow direction circuit. The white arrows indicate the direction of blood flow*

1.2.2. Cardiac Cycle with Pressure Profile

Under one heart cycle the ventricles and the atria contract and relax in two sequential phases. The phase contraction is known as systole, when the heart pumps out the blood from the ventricular chambers to pulmonary arteries and aorta, and the phase relaxation, also known as diastole, when blood flows from the atria to the ventricles. Concisely, during systole the heart chambers eject blood, and during diastole the heart chambers fill with blood. Two consecutive heart cycles are presented in Figure 1.3, where it can be seen that gradients in the pressure curves correspond to the events of heart sounds and ECG that is resulted from the sequential systole and diastole. The constituents of ECG were introduced in the previous subsection while heart sounds' components are described in the next subsection. Cardiac cycle can be understood with the pressure profile which is associated with the mechanical and electrophysiological changes in the heart. The times involved in realizing contraction and relaxation are addressed as systolic and diastolic period, respectively. Thus, a heart cycle is composed by one systolic and one adjacent diastolic period.
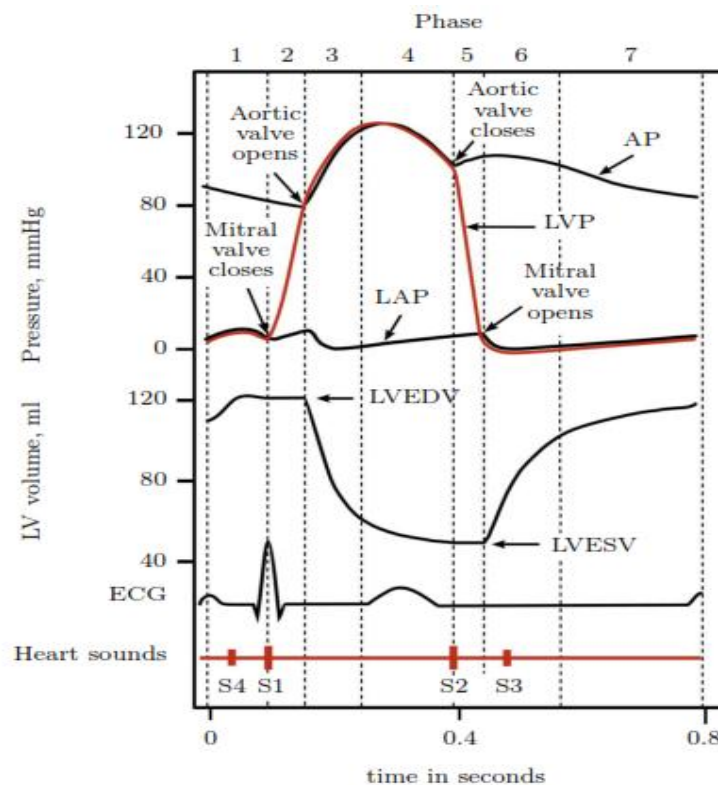
Figure (1.3). [10] *Cardiac cycle phases: (1) atrial systole, (2) is ovolumetric contraction,(3) rapid ejection, (4) reduced ejection, (5) isovolumetric relaxation, (6) rapid filling, and (7) reduced filling, LV: left ventricle, AP: aortic pressure, LVP: left ventricular pressure, LAP: left atrial pressure, LVEDV: left ventricular end–diastolic volume, LVESV: left ventricular end–systolic volume.*

1.3. Digital Auscultation

Cardiac auscultation is known to have been practiced during the Hippocratic period (460 to 370 BC) [11]. At that time, until the nineteenth century, auscultation was performed by pressing the hand or the hearing against the patient's body, a process known as immediate auscultation. Only in 1816 did a french physician named Rene Laennec discover the stethoscope when faced with difficulties when examining a fat patient. Based on simple acoustics, he decided to roll a paper into a sort of cylinder which allowed him to better listen to heart sounds [11]. His discovery gave rise to a number of developments in cardiology and the stethoscope has since then evolved into a high precision instrument used commonly in every hospital. With the advent of new technology in the twentieth century, which brought to light other sophisticated diagnostic modalities such as echocardiography and chest x-rays, phonocardiography, the diagnostic technique that creates and studies a graphic record of heart sounds, became less important. The decline of auscultation teaching in medical schools and a consequent lack of confidence and accuracy in identifying heart sounds and murmurs also contributed to this fact [12]. However, with the evolution of computers and digital signal processing, phonocardiograms (PCGs) may reveal important information [13]. Traditional mechanical stethoscopes possess certain limitations in what concerns the study of the PCG: they cannot store and playback sounds, cannot offer a visual display nor process the acoustic signal. In order to overcome the limitations of these mechanical tools, electronic stethoscopes have been developed. Nowadays, with the advent of miniaturized and powerful technologies for computing, these limitations are rapidly receding [11] and electronic and digital stethoscopes are being used in areas such as telehealth [12], phonocardiography [13], among others.

1.3.1 Auscultation areas

Perception of heart sounds is influenced by their production and transmission as well as the capability of the human auditive sensory system in recognising correct amplitude and frequency of each sound. The human ear is not equally responsive to sound in all frequency ranges, and has a relative perception about loudness and softness of a sound. Two sounds with the same intensity at different frequencies are perceived differently. The human ear has an optimal sensitivity range between 1 and 5 kHz. This frequency range is perceived louder than an equally intense, but lower frequency sound (e.g., 200 Hz) because of the ear's poor sensitivity in the lower frequency range [14]. Auditory performance of a human being is limited and requires adapted devices to achieve better cardiac auscultation.
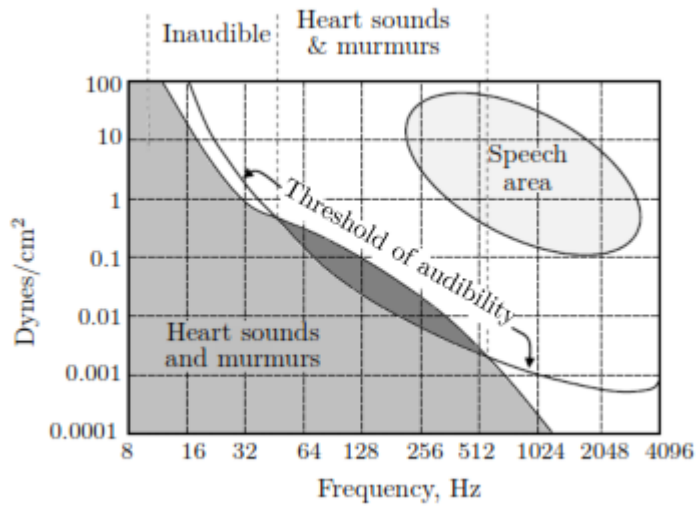
Figure (1.4). *Audibility of heart sounds and murmurs*

The other hand the technique of deciphering the sounds of the body based on their intensity, frequency, duration, number and quality is called auscultation [15]. The acoustic signal is affected by a chain of transfer functions before the physician's actual decision-making process starts. The signal transmitted from the sound source propagates through the human body, where the sound waves are both reflected and absorbed. The most compressible tissues such as lung tissue and fat contribute most to the absorption. Low frequencies are less attenuated compared to high frequencies, but the high frequencies are easier to perceive.

AUSCULTATORY AREAS
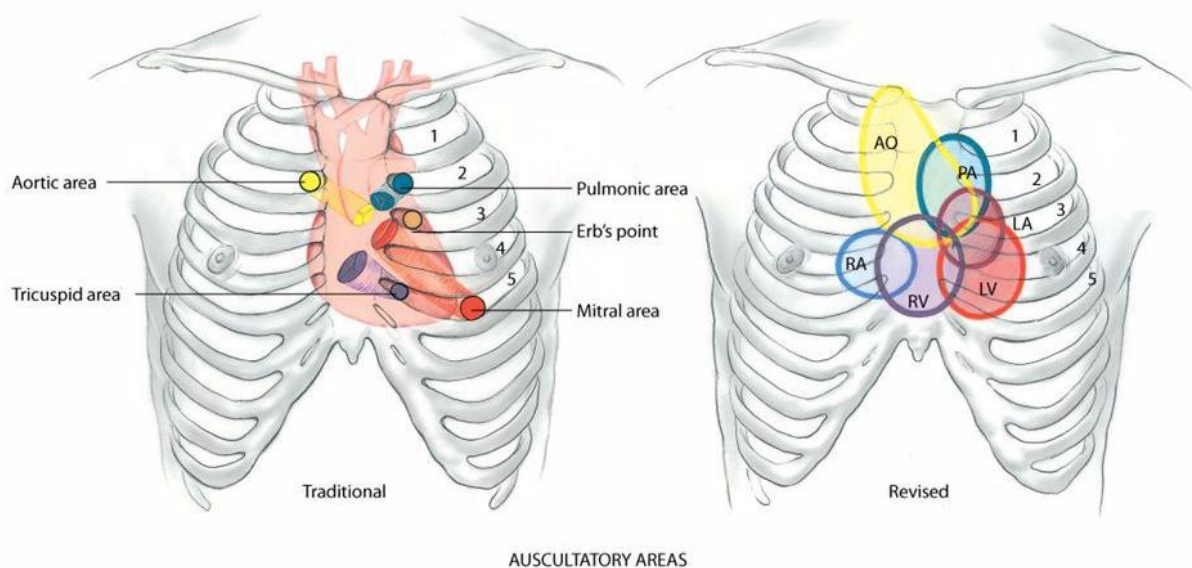
Figure (1.5).*The traditional auscultatory areas on the chest*

The consequences of the attenuation are therefore hard to predict. To reduce the effect of thoracic damping, certain areas of cardiac auscultation have been defined. In these locations, as shown in Figure 1.5, the sound is transmitted through solid tissues or through a minimal thickness of lung tissue. The traditional areas of auscultation where the radiated sound intensity from each of the four heart valves is maximized and are described below by .

• **Mitral area:** The cardiac apex.

• **Tricuspid area:** The fourth and fifth intercostal space along the left sternal border.

• **Aortic area:** The second intercostal space along the right sternal border.

• **Pulmonic area:** The second intercostal space along the left sternal border.

1.3.2 Electronic stethoscope

Based on the technology provided by digital stethoscopes, a tool for collecting, storing and processing acoustic auscultation signals has been created. The DigiScope collector [16] was developed with the immediate goal of creating a repository of annotated auscultation signals for biomedical signal processing and machine learning research. This repository has been the testing ground for the work developed during this thesis and will henceforth be referred to as Digi-Scope repository. Figure 1.6 shows the DigiScope collector with a Littmann Model 3200 digital stethoscope, used to record and transmit heart sounds.

Figure (1.6). *The DigiScope Collecto hardware prototype. It has unrivalled acoustic performance of 24x magnification with 85 percent of the noise reduction for friction and ambient noise.*

Using the capabilities of a digital stethoscope to record and transmit heart sounds will allow this software application to be used as a transmission tool for professionals to discuss diagnoses together, as a teaching tool for medical students, or as a method for screening cardiac pathology by using signal processing and machine learning computational resources.

1.3.3 Noise reduction in digital stethoscopes

Auscultation now uses digital stethoscopes and concerns with the automated acoustic recording and processing of medical signals. But these medical signals can potentially be corrupted by noise in a variety of ways. The sequence of corruption demonstrates several key areas where external interferences could cause degradation of the original signal. When dealing with critical medical signals, such as heartbeats, it is important if the data does become corrupted by noise and these alterations can be eliminated in an accurate and effective manner.

1.3.4 Noise analysis

In reality, heart sound records are often disturbed by various factors, which can prohibit the accuracy of the original sound. Most of these factors are noises from sources such as breath sounds, contact of the stethoscope with the skin, fetal heart sounds if the subject is pregnant and ambient noise that may corrupt the heart sound signals. To make it easier, these factors can be categorized as two aspects in the mass: external factors and internal factors.

External factors:

- Small movement of the stethoscope ("shear noises" or friction noises)
- Ambient noise
- Instrument noises
- Human voices
- Patient movements

Internal factors:

- Respiration sounds (lung mechanics) or breathing noise.
- Acoustic damping through the bones and tissues.

Currently, there is no way of knowing a priori what the particular noise component is, or of determining the noise component once the measurement has been recorded.

The electronic stethoscope will become a much more useful diagnostic tool if unwanted noises are removed, revealing the heartbeat sound clearly and integrated. This research attempts to find the suitable way to reduce the unwanted noise and improve the quality of the heart sound.

1.3.5 Similar phonocardiogram

Phonocardiogram or PCG is a high fidelity technique for registering sounds and murmurs made by the heart during a cardiac cycle with the help of phonocardiograph. The sounds are thought to result from vibrations of the heart valves. It allows the detection of the timing and relative intensities of faint sound and murmur, and make a permanent record of these events. In contrast, the conventional stethoscope cannot detect such sounds or murmurs, and provides no record of their occurrence. The ability to quantify the heart sounds provides vital information about the effects of certain cardiac changes in wave shape and timing parameters upon the heart. It is also an effective method for tracking the progress of the patient's disease. Although Phonocardiography can record and store auscultator findings accurately, its usage as a diagnostic tool is uncommon because of critical procedures and complicated instrumentation.

1.4 Sounds of Intracardiac Vibrations

In this section, electronic resources of cardiac auscultation tutorials designed of auscultation training purposes are used to study the various cardiac disorders through their phonocardiographic recordings.

1.4.1 Timing of heart sounds

The heart, during its continuous cyclic beating, generates sounds recorded as phonocardiogram (PCG) signal. The phonocardiogram of a healthy subject can record up to four sounds, which are not all audible (see Figure 1.4). A normal phonocardiogram is usually formed by S1 and S2 sounds during a cardiac cycle. These sounds appear at the onset of the systole and the diastole phases respectively. The sinusal node is closer to the tricuspid valve in comparison to the mitral valve. Consequently, the right atrial contraction leads up to the left one. Therefore, the left and right hearts are not synchronized, as are their generated sounds. Interestingly, the contraction of the left ventricle begins and finishes before that of the right ventricle. These electromechanical events generate sounds appearing at different moments of time during the cardiac cycle. This timing is of great importance in diagnosis assessment.

1.4.2. Heart Sounds

There are two major heart sounds, which are always present, and two less dominant heart sounds, which can be observed only in a restricted group of people. As shown in Fig. 1.7, the first heart sound (S1) is produced at the beginning of the systole, and is caused by the closing of the atrioventricular valves and vibration of the ventricle walls.The second heart

sound (S2) coincides with the end of the systole and beginning of the diastole, and it is generated by the closing of the aortic and pulmonary valves and by the fast deceleration of the arterial blood. The third (S3) and forth (S4) heart sounds occur during the diastole. The S3 sound is believed to be initiated by the sudden deceleration of atrioventricular blood when the ventricle reaches its limit of distensibility, causing vibrations of the ventricular wall. Finally, the S4 sound is produced by the end-diastolic atrial contractions, resulting in vibrations of the ventricle wall like in the case of the S3 sound [17]. The S3 and S4 sounds are rarely observed in the neonatal period. In the case of fetal and preterm heart sound recordings only the S1 and S2 sounds can be detected, due to the low signal-to-noise ratio.
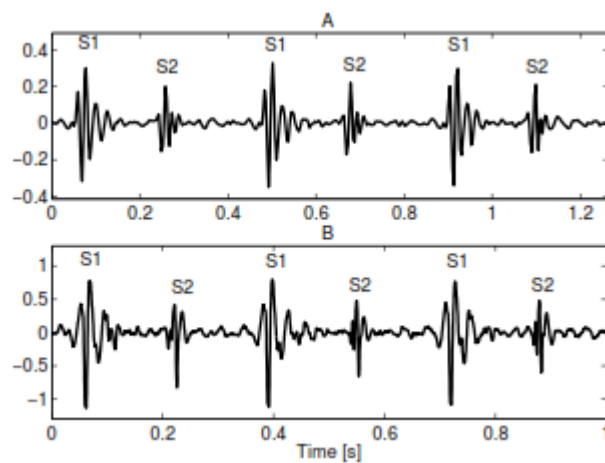
Figure (1.7). *Three heart cycles of typical (A) fetal and (B) preterm neonatal heart sound recordings.*

1.4.3 Heart sound analysis

Heart sound provides clinicians with valuable diagnostic clues and crucial prognostic information with acoustical and mechanical phenomena of the cardiac cycle. As many heart diseases are associated with the characteristic changes in the intensities of or the time relation between the S1 and S2, it is crucial to analysis the frequency range of each heart component to conduct the initial diagnostics. The whole frequency of heart sounds and murmurs is a wide range from 0.1Hz to 2000Hz. However, most of the information carried by the heart signal is too weak to be recognized by the human ear. Thus the audible range of the heart sounds above the audible level is about 40–500 Hz, which possessed only a narrow audible range . The first heart sound (S1) is characterized by higher amplitude, low tone and longer duration in comparison with other heart sounds. S1 has two major high-frequency components and its frequency components are mainly in the range of 10–200 Hz. The second heart sound (S2) usually has a more extended spectral activity compared with the first heart sound (S1). Specifically, S2 spectra have greater amplitude than S1 spectra above 150Hz. It occu-

pies frequencies between 50Hz and 300Hz. Because the frequency range of heart sound is generally certain to some degree, removing the noises outside this range is as easy as introducing the suitable digital filters. However, for those noises contained in the pass band, another method is necessary.

1.4.4. Splitting of heart sounds

A feature which has clinical significance is the splitting of heart sounds. As described earlier, the S1 and S2 sounds are the result of valve closure and vibration occurring on both sides of the heart, which yield two components for both heart sounds. There is usually just a very short delay between the timing of these components producing in general a single heart sound. Nevertheless, if – due to some reason – the closing of the valves happens significantly earlier or later on one side, then this single heart sound will change into two sounds – a split heart sound. The genesis of the S1 is surrounded by some controversy [13, 14]; however, the closing of the atrioventricular valves is beyond all doubt involved in the generation of the first heart sound. The mitral valve closes usually slightly earlier than the tricuspid valve on the right side, but in general they cannot be separated. Splitting of the S1 sound has also important clinical implications. An example of fetal S1 split is shown in Fig. 1.7. It is well supported that the S2 sound is composed of a component produced by the closure and vibration of the aortic valve and surrounding tissues (A), followed by a sound resulting from the closure and vibration of the pulmonary valve and surrounding tissues (P2). The A2 component usually precedes the P component; their temporal separation is denominated as the S2 split. In adults, the separation increases during inspiration up to 80 ms, known as physiological split, due to an increased amount of blood returning to the right ventricle and a decreased amount of blood returning to the left ventricle, which results in a delayed P2 component and an earlier A2 component, respectively. During expiration the splitting decreases again, resulting in the sensation of a single sound. Reversed splitting, that is splitting only during expiration might indicate aortic stenosis or left bundle branch block. On the other hand, splitting during inspiration and expiration is often a symptom of pulmonary stenosis, atrial septal defect or ventricular septal defect.

1.4.5. Abnormal Heart Sound or Heart Murmur

Abnormal heart sounds, or heart murmurs, mainly emerge as a result of a turbulent blood flow by a constriction in the artery or an insufficiently functioning heart valve . Since turbulence is a chaotic dynamic state, the resulting heart murmur differs greatly from the heart sounds which have an oscillating background. Although simulations of flows in cylindrical

tubes with certain constrictions give new insight into the dynamics behind heart murmur, there is still a great lack of understanding, which hinders the exploitation of the diagnostic value of heart murmur
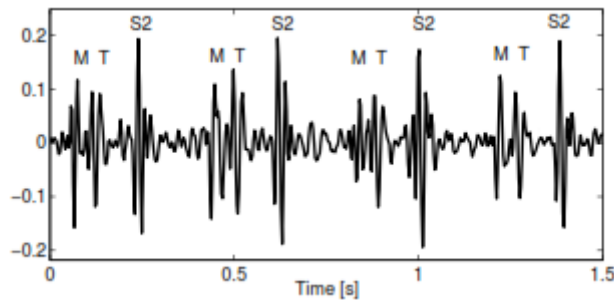
Figure (1.8). *Fetal heart sound record with 60 ms S1 split, separating the mitral (M) and tricuspid (T) component of the first heart sound.*
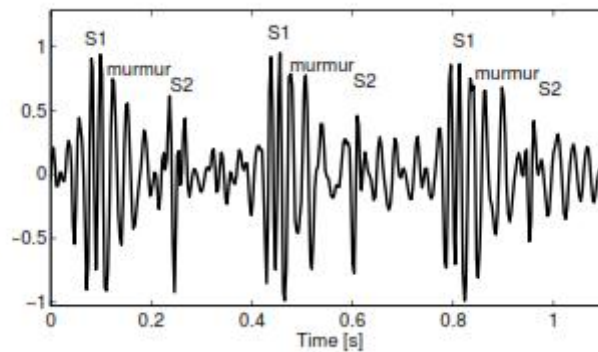
Figure (1.9). *Fetal heart sound record with a significant systolic murmur due to turbulent blood through collateral arteries.*

Although the presence of murmur is always related to some deviation resulting in turbulent blood flow, if the real cause is hemodynamically insignificant, it is regarded as innocent murmur. In contrast, murmur related to some cardiovascular disease is called pathological murmur [15]. Usually five properties of heart murmur are assessed during auscultation in clinical practice [16]:

- **Timing and duration:** murmurs should be identified as being systolic or diastolic (or rarely, continuous). The duration can then be subdivided into further subcategories, such as early, mid, late systolic or even holosystolic.

- **Intensity:** the intensity of a murmur is graded on a scale of 1-6, where grade 1 is a quiet murmur that can be heard only after careful auscultation over a localized area and grade

6 is a murmur sufficiently loud to be heard with the stethoscope raised just off the chest surface.

- **Point of maximal intensity and radiation:** point of maximum refers to where the murmur can be heard well. Several locations on the chest are defined which correspond to specific parts of the heart. Regarding the radiation, a general rule of thumb is that the sound radiates in the direction of the blood flow.

- **Shape:** the shape describes the intensity change of the murmur during the cardiac cycle and it is related to the corresponding ow velocities. It is described by musical notions, for example crescendo or decrescendo, but the intensity can also remain fairly constant.

- **Character:** it is described by the pitch of the murmur and based on the spectral configuration. For example, in the case of a musical murmur typically a dominant tone is present, but usually many frequencies build up the murmur, making it blowing, harsh, or rumbling. However, in Cardiac murmurs are vibrations caused by turbulence in the blood as it flows through some narrow tube. A murmur is one of the more common abnormal phenomena that can be detected with a stethoscope - a somewhat prolonged "whoosh" that can be described as blowing, rumbling, soft, harsh, and so on. Murmurs are sounds related to the non-laminar flow of blood in the heart and the blood vessels. They are distinguished from basic heart sounds in that they are noisy and have a longer duration. While heart sounds have a low frequency range and lie mainly below 200 Hz, murmurs are composed of higher frequency components extending up to 1000 Hz. Most heart murmurs can readily be explained on the basis of high velocity flow or abrupt changes in the caliber of the vascular channels.

The Table 1.1 summarizes various types of heart sounds and murmurs with unique perceptual features that distinguish from other murmurs. Doctors use these perceptual features (e.g., gushing sound with high pitch, spilt sounds etc.) and play significant role auscultation. The perceptual features carry significant clinical information that can be used for the clinical diagnosis and cardiovascular treatments.

Table 1.1. Murmurs and their psychoacoustic or perceptual features.

Heart sound or murmurs	Sound/acoustic properties
Aortic Stenosis (AS)	High pitch, high energy envelope
Mitral Regurgitation (MR)	High pitch, high energy envelope with clear
Third Heart Sound (TS)	Faint heart sound after second heart sound
Fourth Heart Sound (FS)	Faint heart sound after third heart sound
Early Systolic Murmur (ESM)	Systolic, early cycle of S1, high pitch, high freq
Late Systolic Murmur (LSM)	Systolic, late cycle of S1 or S2, high pitch, high freq
Ejection Click (EC)	High energy pulse of 2-5 ms
Diastolic Rumble (DR)	Rubbing sound
Atrial Septal Defect (ASD)	Gushing sound with high pitch
Patient Ductus Arteriosus (PDA)	Gushing sound with low pitch and inaudible
II Heart Sound Split (2SS)	Clear split sound of duration 2- 48 ms after s1
III Heart Sound Split (3SS)	Clear split sound of duration 5 - 50 ms after s2
Diastolic Summation Gallop (DSG)	Galloping sound
Diastolic Tricuspid Stenosis (STS)	High pitch and rhythmic
Diastolic Ventricular Gallop (SVG)	Galloping with high intensity & reducing with time
Ejection Murmur (EM)	High intensity and high pitch ejection sound

Heart murmurs have various shapes and timing during the cardiac cycle. Indeed, a heart murmur can occur in systole (*e.g.* systolic in aortic stenosis and mitral regurgitation) or in diastole (*e.g.* aortic regurgitation and mitral stenosis). Heart murmurs can also be continuous such for patent ductus arteriosus.

(i)   Systolic Murmurs

Systolic murmurs may be categorized as mid systolic ejection or pansystolic regurgitant. Although any single categorization has serious deficiencies, the classification popularized by Leatham is attractive because it has a physiologic as well as a descriptive basis [17]. Systolic ejection murmurs are due to flow across the left or right ventricular outflow tract, whereas systolic regurgitant murmurs are due to retrograde flow from a high-pressure cardiac chamber to a low-pressure chamber. Since, the systolic ejection murmur begins shortly after pressure in the left or right ventricle exceeds aortic or pulmonic diastolic pressure sufficiently to open the aortic or pulmonic valve. The result is a delay between $1, which occurs shortly after atrioventricular pressure crossover, and beginning of the murmur (see Figure 1.10). The intensity of an ejection murmur closely parallels changes in cardiac output. Any condition that increases forward flow, such as exercise, anxiety, fever, or increased stroke

volume associated with the long diastolic filling period after a premature beat, increases murmur intensity.
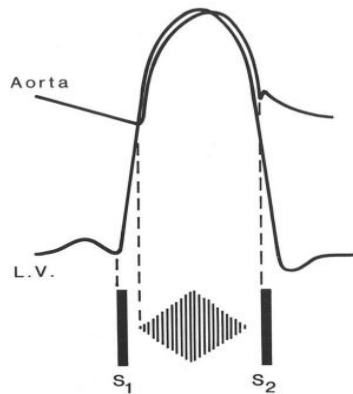
Figure (1.10**).** *Midsystolic ejection murmurs occur during ventricular ejection. As a result, onset of murmur is separated from first heart sound ($1) by period of isometric contraction, and murmur, which is crescendo-decrescendo in nature, stops before respective semilunar valve closure. LV, left ventricle; $2, second heart sound*

❖ **Pansystolic Regurgitant Murmurs**

Pansystolic regurgitant murmurs are produced by retrograde flow from a high-pressure chamber to one of lower pressure [17]. Mitral regurgitation, tricuspid regurgitation, and ventricular septal defect murmurs are classic examples. Since there is usually a high pressure differential between the two chambers throughout systole, the murmurs are holosystolic in duration, high-pitched and blowing in quality, with a plateau-like configuration. Pansystolic regurgitant murmurs begin with $1 and continue up to and through the aortic closure sound
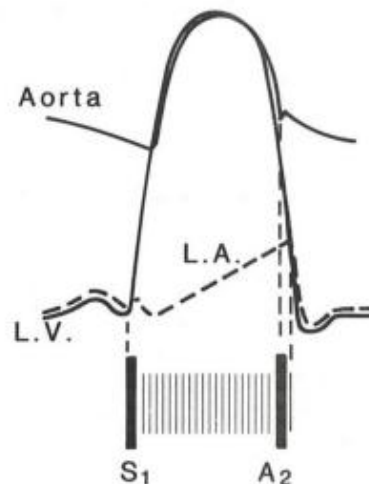
Figure (1.11**).** *Pansystolic regurgitant murmur of mitral regurgitation begins with and may replace first heart sound ($1). This murmur continues up to and through aortic valve closure sound (A2), as ventricular pressure continues to exceed left atrial (LA) pressure. Murmur has plateau configuration and varies little with respiration. LV, left ventricle.*

❖ **Variants of the Pansystolic Regurgitant Murmur**

▪ *Early Systolic Regurgitant Murmurs*: a regurgitant murmur may be confined to early systole, as in the presence of a small ventricular septal defect. This murmur begins in the usual manner, at the onset of ventricular systole, and stops suddenly in early or midsystole [18,19]. The murmur ceases because ventricular size decreases as ejection continues, and the small defect is sealed shut as the ventricular septum thickens during systole, resulting in cessation of flow through the defect. This murmur is important because it is typical of the type of ventricular septal defect that may disappear with age.

▪ *midsystolic and late systolic regurgitant murmurs:* Midsystolic murmurs can occur with mitral regurgitation due to papillary muscle dysfunction [20]. The timing of this murmur may also be late systolic, and may be intermittent or constant. These murmurs are often transient and provoked by episodes of ischemia. Mitral valve prolapse is the most frequent cause of late systolic murmurs; indeed, this entity is one of the most common causes of systolic murmurs seen in clinical practice. It is best heard at the apex and often has a tendency to crescendo in late systole (see Figure 1.12)

Variants of the Pansystolic Regurgitant Murmur
Pansystolic Murmur
Mitral Regurgitation Tricuspid Regurgitation Ventricular Septal Defect
Early Systolic Murmur
Small Ventricular Septal Defect
Acute Mitral Regurgitation
Late Systolic Murmur
Mitral Valve Prolapse   Papillary Muscle Dysfunction

Figure (1.12**).** *In addition to classic pansystolic regurgitant murmur seen in mitral regurgitation, tricuspid regurgitation, and ventricular septal defect, variations exist. In patients with small ventricular septal defects, murmur that starts with first heart sound ($1) may suddenly stop during early or midsystole, purportedly because ventricular volume becomes smaller after maximal ejection, defect seals shut, and murmur ceases. In acute mitral regurgitation, regurgitant murmur may end well before aortic valve closure sound as a result of extremely high left atrial V wave, which abolishes left ventricular-left atrial pressure gradient during late systole. $1 may be soft if flail mitral leaflet is present and is preceded by prominent fourth heart sound ($4). Audible expiratory splitting with accentuated pulmonic valve closure sound is present. Midsystolic to late systolic regurgitant murmurs may be due to papillary muscle dysfunction and prolapse of mitral or tricuspid valve. In latter conditions, valve is competent in early systole, but as ventricular volume decreases, leaflets become incompetent and murmur begins, building in late systole and becoming maximal at time of second heart sound ($2).*

(ii) **Diastolic Murmurs**

Diastolic murmurs have two basic mechanisms of production: Diastolic filling murmurs or rumbles due to forward flow across the atrioventricular valves and diastolic regurgitant murmurs due to retrograde flow across an incompetent semilunar valve [17].

Diastolic rumbles are caused by forward flow across the atrioventricular valves, and their onset is delayed from their respective closure sounds by isovolumic relaxation. Following this period, when atrial pressure exceeds the declining ventricular pressure, the atrioventricular valves open and filling begins. The two phases of rapid ventricular filling are early diastole and presystole. These murmurs tend to be more prominent during these two filling periods. Because flow velocity is relatively low, these murmurs have low-frequency content and rumble.

Diastolic Filling Murmur (Rumble)
Mitral Stenosis

Figure (1.13). *In mild mitral stenosis, diastolic gradient across valve is limited to two phases of rapid ventricular filling in early diastole and presystole. Rumble occurs during either or both periods. As stenotic process becomes severe, large gradient exists across valve during entire diastolic filling period and rumble persists throughout diastolic filling period. As left atrial pressure becomes higher, time from aortic valve closure sound (A2) to opening snap (OS) shortens. In severe mitral stenosis, secondary pulmonary hypertension results in louder pulmonic valve closure sound (P2) and splitting interval usually narrows. S1, first heart sound; S2, second heart sound.*

When the aortic valve becomes incompetent during diastole, a blowing, high-pitched diastolic murmur ensues. Isovolumic relaxation of the ventricle is very rapid. A high gradient quickly develops between the aorta and the left ventricle, and the murmur builds to maxi-

mum intensity almost instantaneously. Thereafter, as the gradient between the two chambers slowly falls, the murmur is decrescendo up to the next S1. The murmur of aortic regurgitation characteristically has the highest pitch of the commonly heard cardiac murmurs and lies in the frequency range to which the ear is most sensitive.

Early Diastolic Murmur		
aortic regurgitation Pulmonic regurgitation (with pulmonary hypertension)		
Organic pulmonary regurgitation (without pulmonary hypertension)		

Figure (1.14**).** *In aortic regurgitation or pulmonic regurgitation secondary to pulmonary hypertension, murmur begins almost simultaneously with second heart sound ($2). Since gradient between aorta and left ventricle is maximal almost instantaneously and then slowly decreases, murmur is also high-pitched, slow decrescendo. In contrast, organic pulmonary regurgitation without pulmonary hypertension is manifested by murmur that starts later and has rapid crescendo with longer decrescendo. This murmur is lower pitched than usual early diastolic blowing murmur because regurgitant flow is across lower pressure system with small gradient. $1, first heart sound.*

(iii)   Continuous Murmurs

A continuous murmur is defined as one that begins in systole and extends through $2 into part or all of diastole [20]. It need not last the entire cycle; therefore, a systolic murmur that extends into diastole without stopping at $2 is considered continuous, even if it fades completely before the subsequent $1.

Continuous Murmur

Figure (1.15**).** *During abnormal communication between high-pressure and low-pressure systems, large pressure gradient exists throughout cardiac cycle, producing continuous murmur.*

(iv)   Innocent murmurs

Innocent murmurs are always systolic ejection in nature and occur without evidence of physiologic or structural abnormalities in the cardiovascular system when the peak flow velocity in early systole exceeds the murmur threshold [18]. These murmurs are less than grade 3 in intensity and vary considerably with body position, level of activity, and fr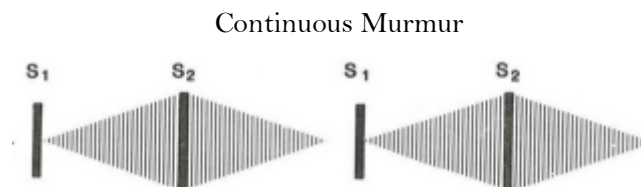om one examination to the next. They are not associated with a thrill or radiation to the carotid arteries or axilla. They may originate from flow across either the normal left or right ventricular outflow tract and always end well before semilunar valve closure. Innocent murmurs are found in approximately 30-50% of all children; the vibratory systolic (Still's) murmur is common, especially in children aged 3-8 years. It has a very distinct quality described as groaning, croaking, buzzing, or twanging and is heard best along the left sternal border at the third or fourth interspace. It disappears at puberty. Although its exact cause is controversial, most authorities agree that this murmur originates from flow across the left ventricular outflow tract. Innocent murmurs have also been attributed to flow across a normal right ventricular outflow tract and are called innocent pulmonic murmurs because the site of their maximal intensity is heard best in the pulmonic area at the second left interspace, with radiation along the left sternal border. These are low to medium pitched, with a blowing quality, and are common in children, adolescents, and young adults. In adults over 50, innocent murmurs due to flow across the left ventricular outflow tract are often heard and may be of high frequency, with a musical quality. They are frequently auscultated best at the apex. Since both innocent and pathologic ejection murmurs have the same production mechanism, it is not the nature of the murmur itself that allows the differential diagnosis but rather associated cardiac findings. Thus, it is the company the murmur keeps that allows the differential diagnosis from the pathologic systolic ejection murmur; the innocent murmur must occur during an otherwise normal cardiovascular examination [21] (see Figure 1.16).

Differential Diagnosis of the Innocent Murmur			
CONDITION	**EXPIRATION**	**INSPIRATION**	**NOTES**
Innocent Cardiac Murmur			Physiologic $3 sometimes present
High Output State			Loud St;S3 and $4 often present
Atrial Septal Defect			Loud Tt ; wide, fixed splitting of $2; tricuspid flow rumble sometimes heard in diastole
Mitral Valve Prolapse			Midsystolic click followed by murmur
Mild Valvular Aortic Stenosis			Loud aortic valvular ejection sound and A2; soft AR murmur commonly present in diastole
Mild Valvular Pulmonic Stenosis			Pulmonic valvular Ejection sound loud on expiration only; wide physiologic splitting of $2
Hypertrophic Cardiomyopathy			Paradoxical splitting of $4 commonly heard

Figure (1.16). *Differential diagnosis of innocent murmur versus pathologic systolic murmur by the company the murmur keeps. Innocent murmur must be found in otherwise normal cardiovascular examination. $1, first heart sound; $2, second heart sound; $3, third heart sound; S4, fourth heart sound; A2, aortic valve closure sound; P2, pulmonary valve closure sound; T1, tricuspid valve closure sound; M1, mitral valve closure sound; C, midsystolic nonejection sound; AVES, aortic*

1.5 Conclusion

This chapter introduced some background information on the cardiac structure, the origin of heart sounds, their characteristics and their diagnostic value, but these medical signals can potentially be corrupted by noise in a variety of ways.

At the start of this chapter, the anatomy and physiology of heart sound was explained in which the structure of the heart and its function, i.e. pumping blood to the body, were described. Then, the origin of and the important characteristics of the main heart sounds' constituents, S1, S2, S3 and S4, were highlighted. Since, Abnormal heart sounds are originated because of some cardiovascular anomalies, namely in valvular diseases, have been explained

Chapter 2
Wavelet Transforms for signals

2.1 Introduction

Physiological of biomedical signals are mostly non-stationary such as phonocardiogram (PCG) and electroencephalogram (EEG) and electromyography (EMG) signals . Addition to the main difficulty in dealing with signal processing is the extreme variability of the signals and the necessity to operate on a case by case basis. The Wavelet transform (WT) has been extensively used in signal processing, mainly due to the versatility of the wavelet tools. It has been shown to be a very efficient tool for analysis of non-stationary and fast transient signals due to its good estimation of time and frequency (scale) localizations.

2.2 Wavelet History

The development of wavelets can be linked to several works in different domains, starting with the first wavelet introduced by Haar in 1909. In 1946, Denis Gabor, introduced the Gabor atoms or Gabor functions, which are functions used in the analysis, a family of functions being built from translations and modulations of a generating function. In 1975, George Zweig, former particle physicist who had turned to neurobiology, has discovered the continuous wavelet transform (named first the cochlear transform and discovered while studying the reaction of the ear to sound). Morlet, studying reflection seismology observed that, instead of emitting pulses of equal duration, shorter waveforms at high frequencies should perform better in separating the returns of fine closely-spaced layers. Grossmann, who was working in theoretical physics, recognised in Morlet's approach some ideas that were close to his own work on coherent quantum states. In 1982, Grossmann and Morlet have given the formulation of the Continuous Wavelet Transform. Yves Meyer recognized the importance of this fundamental mathematical tool and developed this theory with collaborators as Ingrid Daubechies and Stéphane Mallat .

2.3 Continuous Wavelet Transform (CWT)

There are different ways to explain the wavelet transform. This goal is in general achieved by introducing the Fourier theory at the beginning. In practice, signals are represented in time amplitude format in the time domain. However, for most signals processing applications, There is a need for other representations as some important information are hidden in the frequency content of the signal. A Fourier Transform (FT) decomposes the signal into complex exponential functions at different frequencies in order to get the frequency content of the signal as in [22]:

$$X(\omega) = \int_{-\infty}^{+\infty} x(t)\, e^{-j\omega t} dt \qquad\qquad (2.1)$$

The integration covers all time instances from minus infinity to plus infinity. Therefore the frequency component ω is equally reflected in the result of the integration, whenever it occurs over time. Simply, the integration won't change whether the frequency component f appears at time t1 or time t2. This makes the Fourier Transform unsuitable for non-stationary signal whose frequency content changes over time. The signal is supposed to have the frequency component w at all times in a way that the Fourier transform will turn to be useful. Therefore the stationary and the non-stationary nature of the signal is of importance to the FT. It is then natural that a transform with both time and frequency localisation is required for non-stationary signals. The short time Fourier transform (STFT) falls into this category of transforming. There is only a minor difference between the STFT and the FT. In STFT, the signal is divided into small enough segments, where these segments (portions) of the signal can be assumed to be stationary. For this purpose, a window function "w" is required. The width of this window must be equal to the segment of the signal where its stationarity is valid. The STFT is summarised in one line in equation 2.2.

$$\text{STFT}\{x(t)\} = X(\theta, \omega) = \int_{-\infty}^{+\infty} x(t)w(t-\theta)\, e^{-j\omega t} dt \qquad (2.2)$$

Where x (t) represents the signal under consideration and w(t) the window function. As it can be seen from the equation, the STFT of the signal is the FT of the signal multiplied by a window function. The STFT transform of a signal x(t) is thus defined around a time θ through the use of a sliding window [23]. As it can be seen from equation 2.2, even if the integral limits are infinite, the analysis is always bounded by the limits [-θ , θ] of the sliding window. The combination of time domain and frequency-domain analysis yields a more revealing picture of the signal, showing which spectral components are present in a signal at a given time slot [24]. According to Heisenberg's uncertainty principle, it is not possible to know what spectral components exist at a particular time instance [25]. This leads to some limitations of the STFT. A time interval is necessary to find which specific frequencies occur at this specific time. The time information is limited to the time interval, leading to a low resolution. While a Kernel function being infinite in length leads to perfect frequency resolution (with no time information) in the case of the FT, finite window length in STFT assures no perfect frequency resolution. Moreover, the window used in the STFT should be short enough to assure that the signal is stationary.

The narrower the better is the time resolution and the poorer is the frequency resolution.

The Wavelet Transform is useful if the signal to be processed has high frequency components for a short while and low frequency components for longer time; which is typical of signals. Although the CWT is applied in a similar way as the STFT, there are two main differences: Unlike the STFT, the window function is modified as the transform is computed for every single spectral component. The continuous wavelet transform of a function $x(t)$ at a scale (s) and translational parameter (τ) is defined as

$$X_{WT} = \langle x, \psi_{\tau,s} \rangle = \int_{-\infty}^{+\infty} x(t) \frac{1}{\sqrt{s}} \, \psi^* \left(\frac{t-\tau}{s}\right) dt \qquad (2.3)$$

Where $\psi(t)$ is a continuous function in both time domain and the frequency domain called *the mother wavelet* and $x(t)$ belongs to the square integrable function space, L (R). In the same way, The inverse CWT can be defined as:

$$x(t) = \frac{1}{C_\psi} \int_0^\infty \int_{-\infty}^\infty \frac{1}{\sqrt{s}} \, CWT\psi^* \left(\frac{t-\tau}{s}\right) \frac{dsd\tau}{s^2} \qquad (2.4)$$

The C_ψ factor is crucial for reconstruction purposes which is known as the admissibility condition (Daubechies)[26].

$$C_\psi = \int_0^\infty \frac{|\Psi(\omega)|^2}{\omega} \, d\omega \, < \infty \qquad (2.5)$$

Where $\Psi(\omega)$ is the Fourier transform of $\psi(t)$. In practice, $\Psi(\omega)$ will have sufficient decay, so that the admissibility condition reduces to

$$\int_{-\infty}^{+\infty} \psi(t)dt = \Psi(0) = 0 \qquad (2.6)$$

The time-frequency planes of a STFT and Wavelet Transformation (WT) illustrated in Figure $(2.1), (2.2)$. The difference between the STFT and the WT is visually clear.
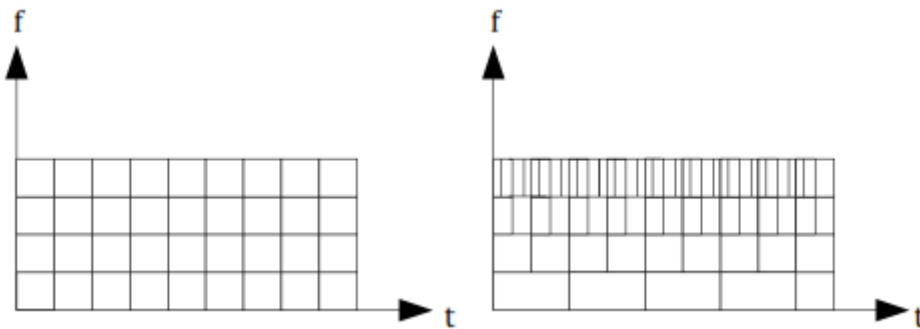
Figure (2.1). *Time-Frequency Structure of STFT. The graph shows that time and frequency localizations are independent. cells are always square.*

Figure (2.2). *Time Frequency structure of WT. The graph shows that frequency resolution is good for low frequency and time resolution is good at high frequencies*

After this brief introduction, let's define what wavelet transforms are. Although a wavelet transform is defined as a mathematical tool or technique, there is no agreed definition on the wavelet transform within the scientific community.

According to Sweldens, three properties have to be fulfilled to call a particular function a wavelet system [27]:

❖ Most of the energy of wavelet is limited in a finite interval and the transform contains frequencies only from a certain frequency band which is called space frequency localization.

❖ Wavelets are building blocks for general functions. Namely, a function is represented in the wavelet space by mean of an infinite series of wavelets.

❖ Wavelets support fast and efficient transform algorithms which are important when implementing the transform.

However, the result of a wavelet transform for one-dimensional signal results in a two-dimensional function depending on the location τ and scale s. In Figure (2.3), the working principle of a wavelet transform is explained.

Figure (2.3). *Representation of the (continuous) wavelet transform*

2.4 Discrete Wavelet Transform (DWT)

The wavelet transform can be computed discretely on the time-frequency plane to reduce the redundancy. The crucial point is how to sample s 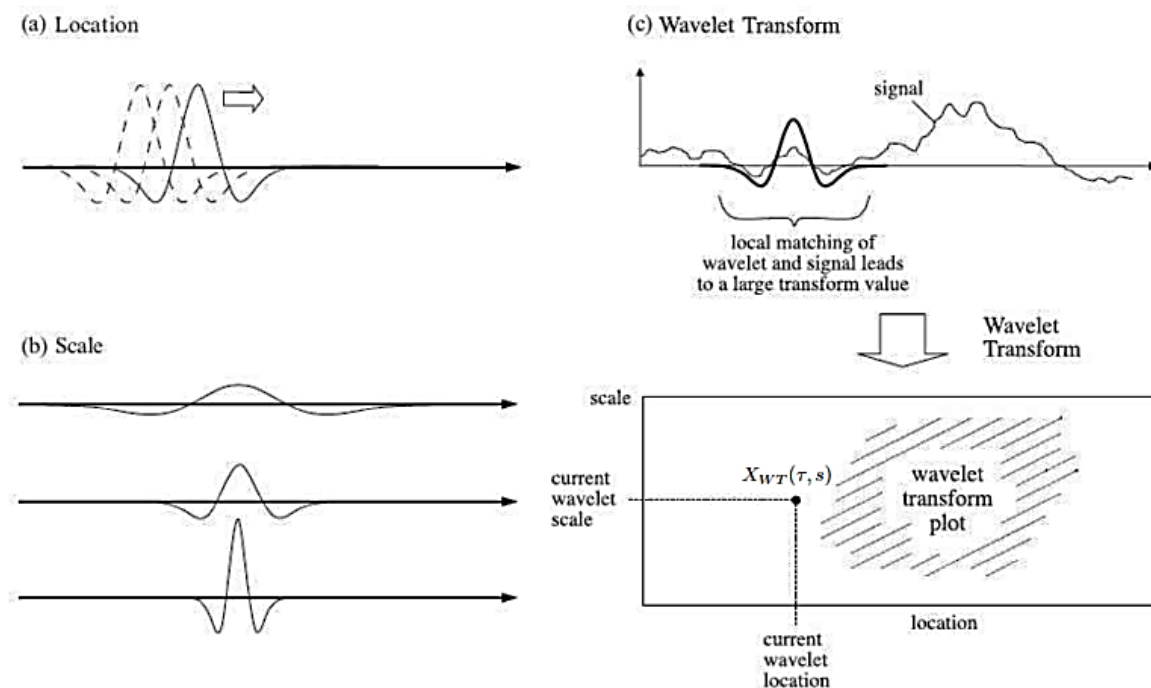and τ to guarantee the precise reconstruction of original signal $x(t)$ from its wavelet transform. There are several forms of wavelet transform according to the different level of discretization. Simply let $s = s_0^j$ and $\tau = n\tau_0 s_0^j$, where s_0 and τ_0 are the discrete scale and translation steps respectively

$$\psi_{j\tau} = \frac{1}{\sqrt{s_0^j}} \psi\left(\frac{t - n\tau_0 s_0^j}{s_0^j}\right) \tag{2.7}$$

The necessary conditions imposed on ψ , s_0 and b_0 for $\psi_{j\tau}, j, n \in Z^2$ to be a frame of $L^2(R)$ is to fulfill the admissibility condition given in equation (2.5) and the theorem (2.1).

Theorem 2.1. ($DAUBECHIES$) [28]. if $\psi_{jn}, j, n \in Z^2$ is a frame of $L^2(R)$ that provides the lower and upper bound for the frame bounds A and B ,where A and B are constants,

$$A \leq \frac{C_\psi}{\tau_0 log s_0} \leq B \tag{2.8}$$

$$\forall \omega \in R - \{0\}, A \leq \frac{1}{\tau_0} \sum_{j=-\infty}^{+\infty} \left|\Psi(s_0^j \omega)\right|^2 \leq B \tag{2.9}$$

The condition (2.9) imposes that the Fourier axis is completely covered by wavelets dilated by $\{s_0^j\}_{j\in Z}$. When τ_0 and s_0 is close to 0 and 1, the functions of the frame are strongly related and behave like continuous wavelet. However, τ_0 and s_0 are chosen to compose an orthogonal basis and hence wavelet series (WS) transform is defined to a continuous mother wavelet ψ and wavelet frames offer good localization both in time and frequency. For 2-D discrete grid of coefficients, $W_\psi: L^2(R) \rightarrow l^2(Z^2)$, The WS transform of a signal $x(t)$ is:

$$W_x(j, n) = \langle x, \psi_{\tau s} \rangle = \frac{1}{\sqrt{s_0^j}} \int_{-\infty}^{+\infty} x(t) \ \psi^*\left(\frac{t - n\tau_0 s_0^j}{s_0^j}\right) dt \tag{2.10}$$

The most commonly used values for s_0 and τ_0 are 2 and 1 respectively. Where the resulting from this particular case of discretization is called the Dyadic Wavelet Transform. DWT of a signal $x(t)$ can be written as:

$$WT_x(j, \tau) = \langle x, \psi_{j,\tau} \rangle = \frac{1}{\sqrt{2^j}} \int_{-\infty}^{+\infty} x(t) \ \psi^*\left(\frac{t - \tau}{2^j}\right) dt \tag{2.11}$$

When a dyadic wavelet transform is discretized in time with a constant interval, $s = 2^j T$,it leads to the classic Discrete Wavelet Transform (DWT). In addition *Meyer* showed that there exist wavelets $\psi(x)$ [29]

$$\left(\sqrt{2^j}\psi(2^j t - k)\right)_{(j,k)\in Z^2} \tag{2.12}$$

is an orthonormal basis of $L^2(R)$ and the wavelet decomposition of signal $x(t)$ is

$$x(t) = \sum_j \sum_k WT_x(j,k)\psi_{j,k} \tag{2.13}$$

The most widely used form of such discretization with $s_0 = 2$ and $\tau_0 = 1$ on a dyadic time-scale grid is shown in Figure (2.4). Such a wavelet transform is described as the standard DWT.
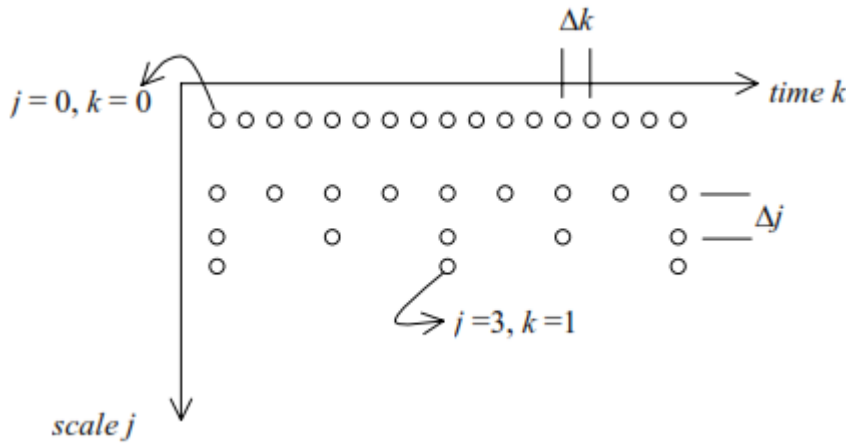
Figure (2.4). *Standard DWT on dyadic time-scale grid*

Several such wavelet bases have been reported in the literature [30-31] to evaluate $x(t)$ using the summation of finite basis over index j and k with finite DWT coefficients with almost no error. All these wavelets can be derived with an arbitrary resolution and with finite DWT co-efficients.. The wavelet orthonormal bases provide an important tool in functional analysis; before them it has been believed that no construction could yield simple orthonormal bases of $L^2(R)$ whose elements had good localization properties in both the spatial and Fourier domains.

2.5 Implementation of DWT

In order to take advantage of the Wavelet Transform's properties, a computation algorithm and an implementation scheme were needed. *Mallat* [32] solved these problems by discussing the Multi-Resolution Analysis (MRA) which is linked to the Perfect Reconstruction (PR) filter bank structures [33].

2.5.1 Multiresolution Analysis (MRA)

A signal's approximation at resolution 2^{-J} is defined as an orthogonal projection on a space $V_j \subset L_2(R)$. The space V_j groups all possible approximations at the resolution 2^{-J} the orthogonal projection of x on V_j is the function x_j that minimizes distance $\|x - x_j\|$. The details of a signal at resolution 2^{-J} are the difference between the approximations at the resolutions 2^{-J+1} and 2^{-J}. However, A multiresolution analysis consists of a sequence of successive approximation spaces $\{V_j\}_{j \in Z}$ resented in Figure 2.5 by the following properties:

$$(i) \quad \forall \in Z, V_j \subset V_{j+1} \tag{2.14}$$

$$(ii) \quad \forall j \in Z, \ x(t) \in V_j \leftrightarrow x\left(\frac{t}{2}\right) \in V_{j+1} \tag{2.15}$$

$$(iii) \ lim_{j \to \infty} V_j = \cap_{j \in Z} V_j = \{0\} \tag{2.16}$$

$$(iv) \ lim_{j \to -\infty} V_j = closure(\overline{\cup_{j \in Z} V_j}) = L_2(R) \tag{2.17}$$
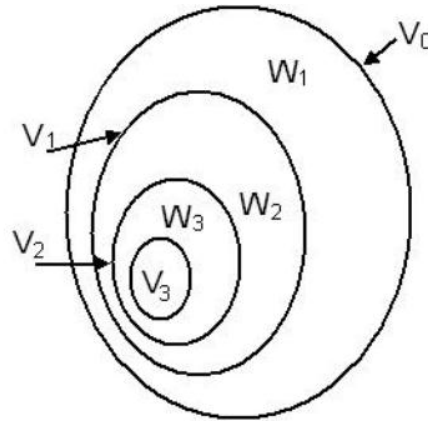
Figure (2.5). *Approximation Spaces V_j and Detail Spaces W_j*

For a given multiresolution approximation $\{V_j\}_{j \in Z}$, there exists a unique function $\emptyset(t)$ $\left(\emptyset_{j,n}(t) = 2^{-j/2}\emptyset(2^{-j}t - n)\right)_{n \in Z}$ is an orthonormal basis of V_j. The orthogonal projection on V_j can be computed by decomposing the signal $x(t)$ in the scaling orthonormal basis. Specifically,

$$\forall x(t) \in L_2(R), pv_i x(t) = \sum_{-\infty}^{\infty} \langle x, \phi_{j,n} \rangle \phi_{j,n}. \tag{2.18}$$

The inner products $\quad a_j[n] = \langle x, \phi_{j,n} \rangle \tag{2.19}$

Hence represent the discrete approximation of the signal $x(t)$ at scale 2^{-j}, It can also be written as :

$$a_j[n] = x * \overline{\phi_j}(2^j n) = \frac{1}{\sqrt{2^j}} \int_{-\infty}^{+\infty} x(t) \ \phi^* \left(\frac{t - 2^j n}{2^j}\right) dt \tag{2.20}$$

Where $\overline{\phi_j}(t) = \frac{1}{\sqrt{2^j}}\phi^*(-2^{-j}t)$.

It can be easily proved that $\overline{\phi_j}(t)$ is the impulse response of a low-pass filter, so, the discrete approximation $a_j[n]$ is a low-pass filtering of x, sampled by a factor of 2^j. The orthonormality condition of the elements of V_0 *is*:

$$\langle \phi_{0,0}, \phi_{0,n} \rangle = \delta(n) \iff \Gamma_\phi(-n) = \delta(n) \tag{2.21}$$

2.5.2 The Detail Signal

The difference of information between the approximations of a signal $x(t)$ at scales 2^{j-1} and 2^j is called the detail signal at scale 2^j. It was shown in the previous paragraph that the approximations of a signal at scales 2^{j-1} and 2^j are equal to its orthogonal projection on V_{j-1} *and* V_j respectively. It can be easily proved that the detail signal at the scale 2^j is given by the orthogonal projection of the original signal on the orthogonal complement of V_j *in* V_{j-1} , denoted here by W_j(see Figure 2.5). If W_j is the orthogonal complement, then $W_j \oplus V_j = V_{j-1}$. Mallat proves in [34] that there exists a function $\psi(t)$, called an orthogonal wavelet, such that, if we denote $\psi_{j,n}(t) = \psi\left(\frac{t-2^j n}{2^j}\right)$ for any scale 2^j, $\{\psi_{j,n}\}_{n \in Z}$ is an orthonormal basis of W_j and $\{\psi_{j,n}\}_{n,j \in Z^2}$ is an orthonormal basis of $L_2(R)$, for all scales. Hence, the detail signal of $x(t)$ at the resolution 2^j is equal to

$$d_j[n] = \langle x, \psi_{j,n} \rangle \tag{2.22} .$$

2.5.3 Filter-bank Implementation of the Discrete Wavelet Transform

As previously mentioned, both approximation and detail coefficients can be obtained by filtering and sub-sampling of the original signal. It is proved that any scaling function is specified by a discrete filter called a 'conjugate mirror filter'. Its impulse response is given by:

$$h[n] = \langle \frac{1}{\sqrt{2^j}}\phi\left(\frac{t}{2}\right), \phi(t-n) \rangle \tag{2.23}$$

Where $\phi(t)$ denotes *the father wavelet* (also known as a scaling function). Its Fourier transform, denoted by $H(\omega)$ is given by:

$$H(\omega) = \sum_{-\infty}^{+\infty} h[n]e^{-j\omega n} \qquad (2.24)$$

With the definitions from above, the following theorem can be introduced:

Theorem 2.2.: $(MALLAT, MEYER)$ [35]

$H(\omega)$ satisfies the following conditions:

$$\forall \omega \in R, |H(\omega)|^2 + |H(\omega + \pi)|^2 = 2 \qquad (2.25)$$

And

$$|H(0)| = \sqrt{2}, \qquad (2.26)$$

Conversely, let $H(\omega)$ be a Fourier transform satisfying (2.25) and (2.26) and such that

$$|H(\omega)| \neq 0 \; for \; \omega \in \left[0, \frac{\pi}{2}\right] \qquad (2.27)$$

The function defined by

$$\Phi(\omega) = \prod_{-\infty}^{+\infty} H(2^{-P}\omega) \qquad (2.28)$$

Where Φ is the Fourier transform of a scaling function.

the filters that satisfy the property (2.25) are called conjugate mirror filters. Relation (2.27) implies that $H(\omega)$ is a low-pass filter. As $\{\phi_{j,n}\}_{n \in Z}$ is an orthonormal basis of V_j any $\phi_{j+1,p} \in V_{j+1} \subset V_j$ can be decomposed as follows:

$$\phi_{j+1,p} = \sum_{-\infty}^{+\infty} \langle \phi_{j+1,p}, \phi_{j,n} \rangle \phi_{j,n} \qquad (2.28)$$

The inner products can be further processed and, taking into account relation (2.24), we obtain:

$$h[n-2p] = \langle \frac{1}{\sqrt{2^j}} \phi\left(\frac{t}{2}\right), \phi(t-n+2p) \rangle \qquad (2.29)$$

Hence

$$\phi_{j+1,p} = \sum_{n=-\infty}^{+\infty} h[n-2p] \, \phi_{j,n} \qquad (2.30)$$

Using (2.19), we can write:

$$a_{j+1}[p] = \langle x, \phi_{j+1,p} \rangle = \sum_{-\infty}^{+\infty} h[n-2p]\langle x, \phi_{j,p} \rangle \qquad (2.31)$$

$$= \sum_{-\infty}^{+\infty} h[n - 2p] a_j[n]$$

$$= a_j[p] * h_d[2p] \qquad (2.32)$$

Where $h_d[n]$ is the reverse filter associated to $h[n]$, $h_d[n] = h[-n]$.

From equation (2.32), we can observe that the approximation coefficients from one iteration can be computed from the approximation coefficients from the previous iteration through low-pass filtering and subsampling with a factor of 2. As previously discussed, orthonormal wavelets carry the details necessary to increase the resolution of a signal approximation. Theorem (2.2) proves that one can construct an orthonormal basis of W_j by scaling and translating a wavelet.

Theorem 2.3:. (*MALLAT, MEYER*) Let ϕ be a scaling function and h the corresponding conjugate mirror filter. Let ψ be the function whose Fourier transform is

$$\Psi(\omega) = \frac{1}{\sqrt{2}} G\left(\frac{\omega}{2}\right) \Phi\left(\frac{\omega}{2}\right) \qquad (2.33)$$

With

$$G(\omega) = e^{-j\omega} H^{\cdot}(\omega + \pi) \qquad (2.34)$$

The necessary and sufficient conditions imposed on G for designing an orthogonal wavelet are:

$$|G(\omega)|^2 + |G(\omega + \pi)|^2 = 2 \qquad (2.35)$$

And

$$G(\omega)H(\omega)^* + G(\omega + \pi)H(\omega + \pi)^* = 0 \qquad (2.36)$$

Where H is a low-pass filter and G is a high-pass filter

From theorem (2.2), we can prove that $G(\omega)$ is the Fourier transform of:

$$g(n) = \langle \frac{1}{\sqrt{2}} \psi\left(\frac{t}{2}\right), \phi(t - n) \rangle \qquad (2.37)$$

which are the decomposition coefficients of

$$\frac{1}{\sqrt{2}} \psi\left(\frac{t}{2}\right) = \sum_{n=-\infty}^{+\infty} g(n)\, \phi(t - n) \qquad (2.38)$$

and

$$g(n) = (-1)^{1-n} h[1 - n] \qquad (2.39)$$

Let us consider $\psi_{j+1,p} \in W_{j+1} \subset V_j$. We can write:

$$\psi_{j+1,p} = \sum_{n=-\infty}^{+\infty} \langle \psi_{j+1,p}, \phi_{j,n} \rangle \, \phi_{j,n} \qquad (2.40)$$

It can be proved that

$$\langle \psi_{j+1,p}, \phi_{j,n} \rangle = \langle \frac{1}{\sqrt{2}} \psi\left(\frac{t}{2}\right), \phi(t - n + 2p) \rangle = g[n - 2p] \quad (2.41)$$

Consequently :

$$\psi_{j+1,p} = \sum_{n=-\infty}^{+\infty} g[n - 2p] \, \phi_{j,n} \qquad (2.42)$$

But the detail coefficients from scale $j + 1$ can be computed with (see also 2.22):

$$d_{j+1}[p] = \langle x, \psi_{j+1,n} \rangle \qquad (2.43)$$

By replacing (2.42) in (2.43) and having in mind relation 2.29, we get:

$$d_{j+1}[p] = \langle x, \sum_{n=-\infty}^{+\infty} g[n - 2p] \, \phi_{j,n} \rangle = \sum_{n=-\infty}^{+\infty} g[n - 2p] \, \langle x, \phi_{j,n} \rangle$$

$$= \sum_{n=-\infty}^{+\infty} g[n - 2p] a_j[n]$$

$$= a_j[p] * g_d[2p] \qquad (2.44)$$

Analyzing (2.44), we can conclude that the detail coefficients from one scale can be computed from the approximation coefficients from the previous scale by convolution with the high-pass reverse filter g_d, $g_d[n] = g[-n]$, followed by a subsampling with a factor of 2.
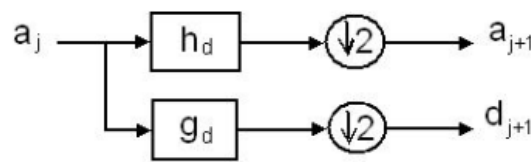

Figure (2.6). *One-level DWT decomposition scheme*

If we consider level 0 as the starting level, namely $x[n] = a_0[n]$. for a three-level decomposition we obtain:
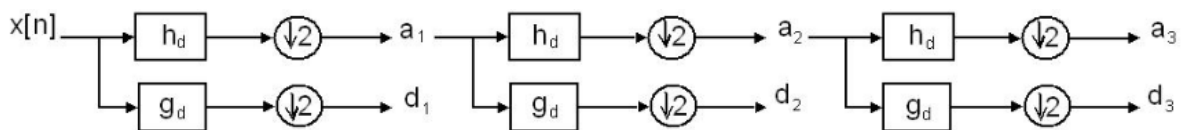

Figure (2.7). *Three level DWT decomposition*

The implementation presented above was first proposed by Stephane *Mallat* and is also called '*Mallat*'s implementation'. Due to the down samplers, the number of coefficients from one scale is equal to the number of approximation coefficients from the previous scale, $(length(a_{j+1}) + length(d_{j+1}) = length(a_j))$.

2.5.4 Perfect Reconstruction

In the reconstruction stage we want to synthesize the original signal from the coefficients obtained in the decomposition stage. This transform is also known as the 'Inverse Discrete Wavelet Transform' (IDWT) .Since W_{j+1} is the orthogonal complement of V_{j+1} in V_j, the union of the two bases $\{\psi_{j+1,n}\}_{n \in Z}$ and $\{\phi_{j+1,n}\}_{n \in Z}$ is an orthonormal basis of V_j. Consequently, any $\phi_{j,p}$ can be decomposed in this basis

$$\phi_{j,p} = \sum_{n=-\infty}^{+\infty} \langle \phi_{j,p}, \phi_{j+1,n} \rangle \phi_{j+1,n} + \sum_{n=-\infty}^{+\infty} \langle \phi_{j,p}, \psi_{j+1,n} \rangle \psi_{j+1,n} \quad (2.45)$$

inserting (2.29 and 2.41) in (2.45) yields

$$\phi_{j,p} = \sum_{n=-\infty}^{+\infty} h[p - 2n] \phi_{j+1,n} + \sum_{n=-\infty}^{+\infty} g[p - 2n] \psi_{j+1,n} \quad (2.46)$$

Using equation (2.56) and the properties of the inner product,we can write the approximation coefficients at level j, $a_j[n]$ as :

$$a_j[n] = \langle x, \phi_{j,p} \rangle \quad (2.47)$$

$$= \sum_{n=-\infty}^{+\infty} h[p - 2n] \langle x, \phi_{j+1,n} \rangle + \sum_{n=-\infty}^{+\infty} g[p - 2n] \langle x, \psi_{j+1,n} \rangle \quad (2.48)$$

$$a_{j+1} * h_r[p] + d_{j+1} * g_r[p] \quad (2.49)$$

Where, $h_r = h, g_r = g$ and with $x[n]$,we have denoted the signal

$$x[n] = \begin{cases} x[p], if \ n = 2p \\ \\ 0, if \ n = 2p + 1 \end{cases} \quad (2.50)$$

This reconstruction can be seen as an interpolation by a factor of 2, that inserts zeros to expand a_{j+1} and d_{j+1}, followed by a filtering of these signals.

In order to achieve perfect reconstruction, one can use orthogonal filters that satisfy

$$|H(\omega)|^2 + |G(\omega)|^2 = 2 \quad (2.51)$$

Theorem 2.4. (*Vetterli*) :The filter bank performs an exact reconstruction for any input signal if and only if

$$H^*(\omega + \pi)H_r(\omega) + G^*(\omega + \pi)G_r(\omega) = 0 \qquad (2.52)$$

and

$$H^*(\omega)H_r(\omega) + G^*(\omega)G_r(\omega) = 2 \qquad (2.53)$$

A one-level reconstruction scheme is presented in Figure 2.8.
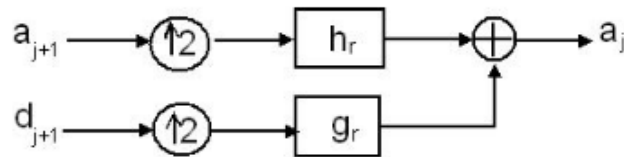
Figure (2.8). *One-level DWT reconstruction scheme*

A three-level reconstruction can be seen in Figure 2.9, where we have considered the approximation at level zero equal to the signal to be reconstructed.
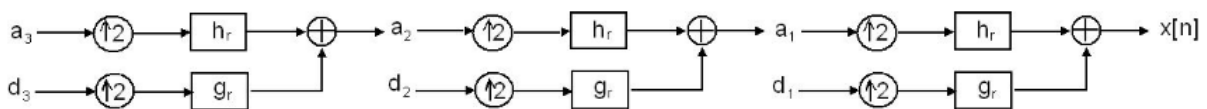
Figure (2.9). *Three-level DWT reconstruction scheme*

2.6 Wavelets for analyzing PCG signals

One of the primary benefits of the wavelet transform is that it is localized in both time and frequency, whereas other classical methods like the Fourier transform are localized in frequency, only.Moreover, the wavelet transform offers good time resolution for low-frequency components and good frequency resolution for high-frequency components of the signal being analyzed. It overcomes shortcomings of other similar methods, such as the short-time Fourier transform, where in time-frequency localization is constant for all frequencies. The result is that a wavelet transform can be designed to detect specific signal transitions localized in time and frequency. CWT is powerful in singularity detection. With standard DWT, signal has a same data size in transform domain and therefore it is a non-redundant transform. Standard DWT can be implemented through a simple filter bank structure of recursive FIR filters. A very important property; Multiresolution Analysis (MRA) allows DWT to view and process different signals at various resolution levels. The advantages such as non-redundancy, fast and simple implementation with digital filters using micro-computers, and MRA capability popularized the DWT for PCG signal denoising

2.7 Basic wavelets and their properties

1. Symmetry and antisymmetry: Since both the scaling function and the mother wavelet can be seen as filters, their phase characteristic plays an important role as the negative derivative of the phase is a group delay. It is very desirable in signal processing application that the filters have a linear phase, thus constant group delay. The linear phase of wavelet filter requires its scaling function to be symmetric or antisymmetric.

2. Orthogonality: This property guarantees the independence of wavelets in time (their shifts and scales), thus some specific kind of exclusivity in signal analysis.

Note that there must always be a trade-off between the orthogonality and symmetry of wavelets, since it is not possible to impose both of them simultaneously.

One of the big issues in research was to design orthogonal wavelets which are symmetric to the degree possible. It is also possible to exploit wavelets which are non-orthogonal, nevertheless, the wavelet theory is then much complicated and is built up on theory of Riesz's bases. Moreover, the wavelet synthesis is not perfect anymore, since there is always an error between original and reconstructed signal.

3. Number of vanishing moments: Some wavelets suppress moment functions, thus polynomial functions of certain order as well. It results in more sparse representation of the wavelet analysis, what can significantly save the memory space while implemented Fugal [2009]. Again, there is a trade-off between number of vanishing moments and the length (dimension) of the wavelets.

4. Existence of scaling function: The simple rule holds about this property: When the scaling function does not exist, the analysis is not orthogonal. Note that the rule is rather theoretical and has no impact on the choice of wavelet family tobe applied in practise, since the (non)orthogonality property of particular wavelet family is always known.

5. Time-frequency localisation: A good localisation of wavelet in either time or frequency determines the possibility of the wavelet to detect particular phenomena in corresponding domain. However, in order to the uncertainty principle, both the compact support and the band-limitations property cannot be attained simultaneously. In other words, the more strict resolution in frequency, the larger support of wavelet, thus the worse time resolution. Analysis in time proceeds by shifting the wavelet along the time axis and analysis in frequency proceeds byscaling the wavelet. Obviously, widening the wavelet shifts its frequency content

towards low frequencies and conversely, narrowing the wavelet shifts its frequency content towards high frequencies.

2.8 Wavelet Families

In general, There are basic properties of a number of common wavelet families. Since,much of this information is drawn from Daubechies [35] and Mohlenkamp and Pereyra [36], but may be found in any standard wavelet reference (for example, Kaiser [37]). The father and mother wavelets of the first few Daubechies wavelets are shown in figure (2.10). Note that the 2 tap Daubechies wavelet is equivalent to the Haar wavelet. Coiflets were created so that the father wavelets has vanished moments too. They are nearly symmetrical and are orthonormal, but have a wide compact support. A Coiflet wavelet family is shown in Figure 2.11. Symlets are a modified version of the Daubechies wavelets, which have maximal symmetry for compactly supported orthogonal wavelets through a wider compact support. A Symlet wavelet family is shown in Figure 212.
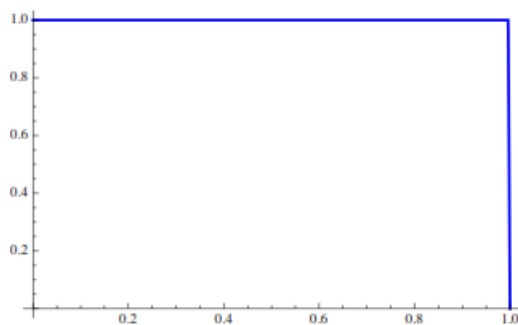
(a) *The Daubechies 2 tap father wavelet*
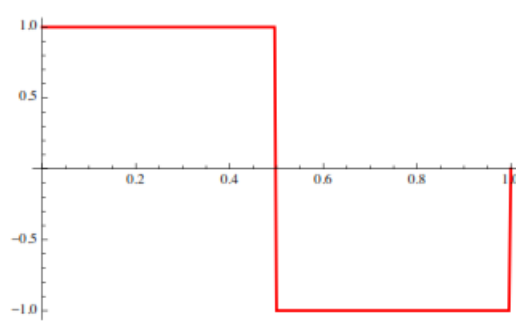
(b) *The Daubechies 2 tap mother wavelet*
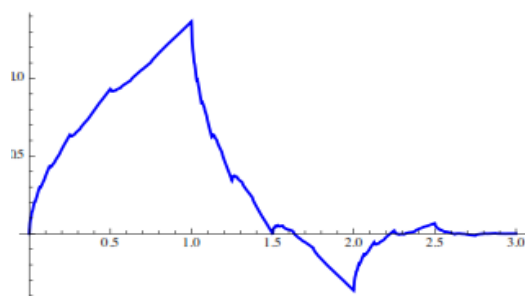
(c) *The Daubechies 4 tap father wavelet*
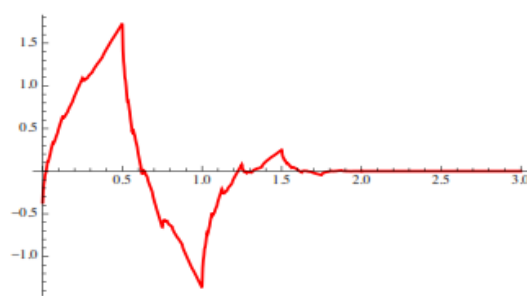
(d) *The Daubechies 4 tap mother wavelet*
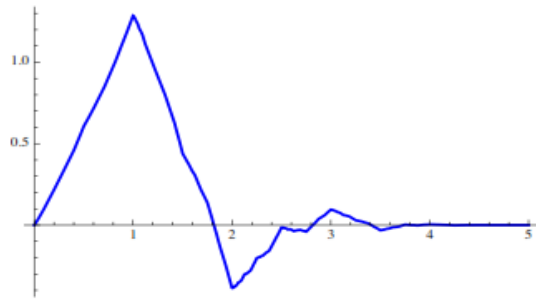
(e) *The Daubechies 6 tap father wavelet*   **(f)** *The Daubechies 6 tap mother wavelet*
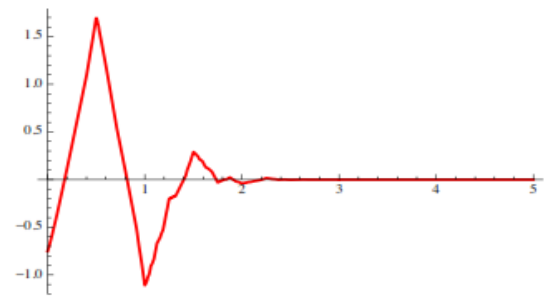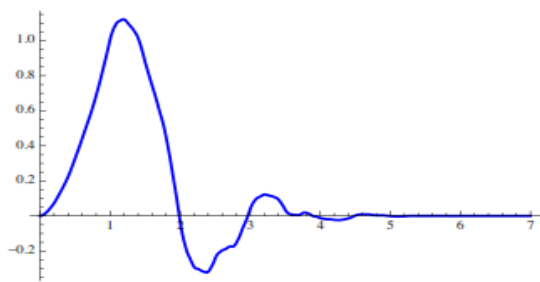
(g) *The Daubechies 8 tap father wavelet*   **(h)** *The Daubechies 8 tap mother wavelet*
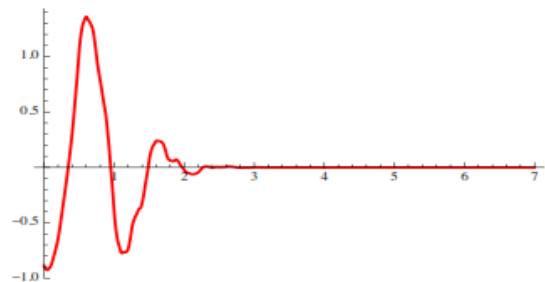
Figure (2.10). *The Daubechies wavelet family.*
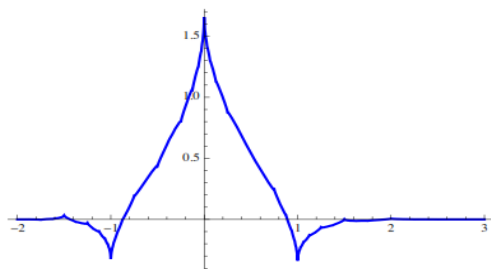
(a) *The Coiflet father wavelet*   **(b)** *The Coiflet mother wavelet*
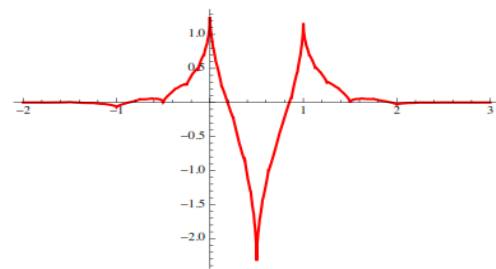
Figure (2.11). *The Coiflet wavelet family*
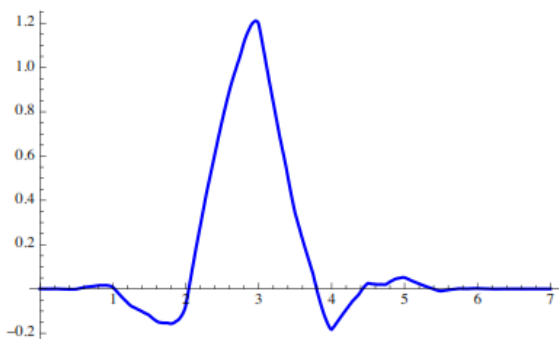
(a) *The Symlet father wavelet*   **(b)** *The Symlet mother wavelet*
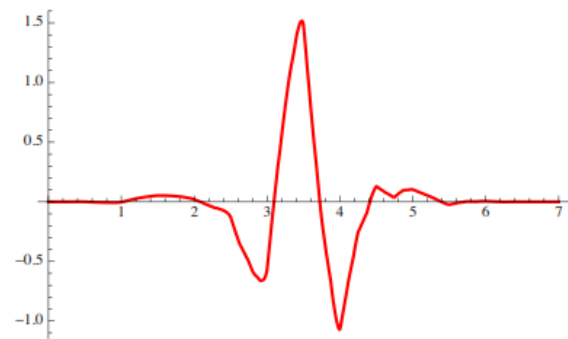
Figure (2.12). *The Symlet wavelet family*

Almost all known orthonormal wavelets, except for the Harr and the Shannon (the sine function), cannot be expressed in closed form or in terms of simple analytical functions, such as the sine, cosine, exponentials, and polynomials. The main feature of wavelets is their natural splitting of objects into different scale components according to the multiscale resolution analysis. However, The discontinuities in the Haar wavelet and poor time localization of the Shannon wavelet have limited their application in the multi-scale modeling. Meyer wavelets are similar to Shannon wavelets, but sacrifice some localisation in frequency to gain exponentially rapid decay. They are shown in Figure 2.14.

(a) *The Shannon father wavelet*   **(b)** *The Shannon mother wavelet*
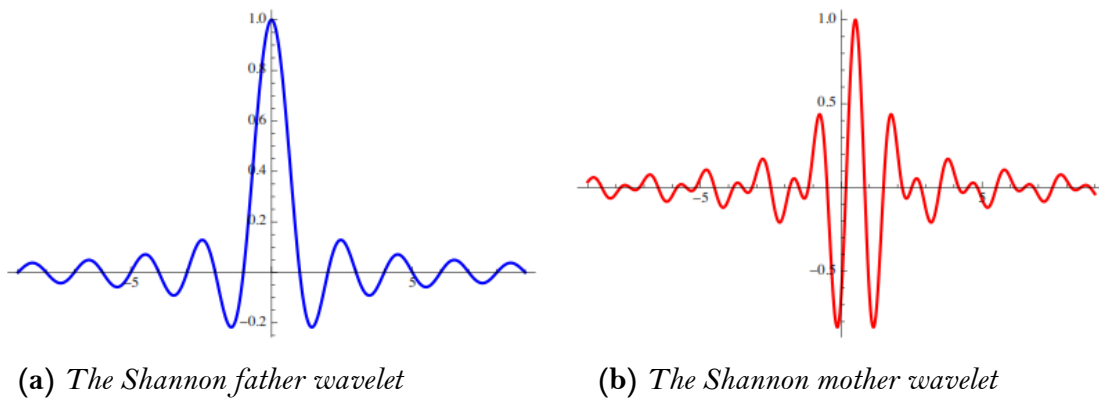
Figure (2.13). *The Shannon wavelet family*

In order to keep the weights equivalent to an inner product a second family of synthesis wavelets orthonormal to the analysis wavelets is used. Weights are computed using the analysis wavelets, and the function can be reconstructed using the synthesis wavelets. While many biorthogonal wavelet families exist, the name usually refers to the Cohen Daubechies-Feauveau (CDF) wavelet [38]. The analysis wavelets of a biorthogonal wavelet family are shown in Figure 2.15, but The synthesis wavelets are in Figure 2.16

(a) *The Meyer father wavelet*   **(b)** *The Meyer mother wavelet*
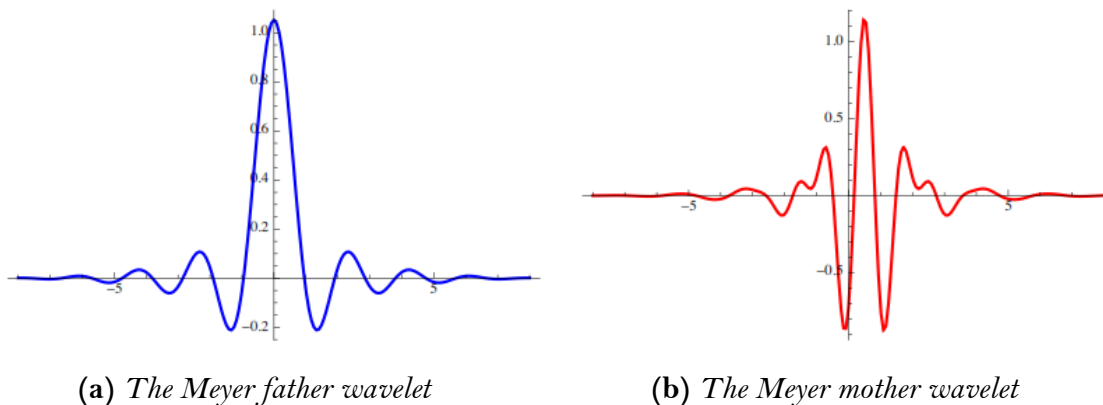
Figure (2.14). *The Meyer wavelet family*
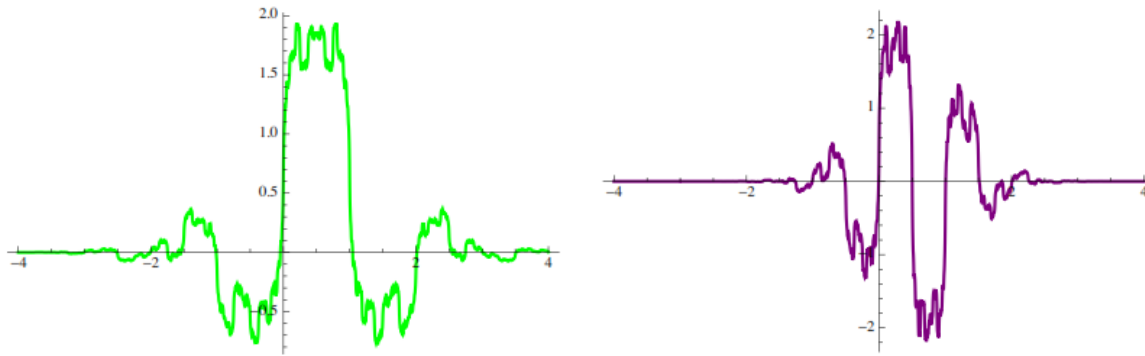
(a) *A biorthogonal father wavelet*   **(b)** *A biorthogonal mother wavelet*

Figure (2.15). *A biorthogonal analysis wavelet family*
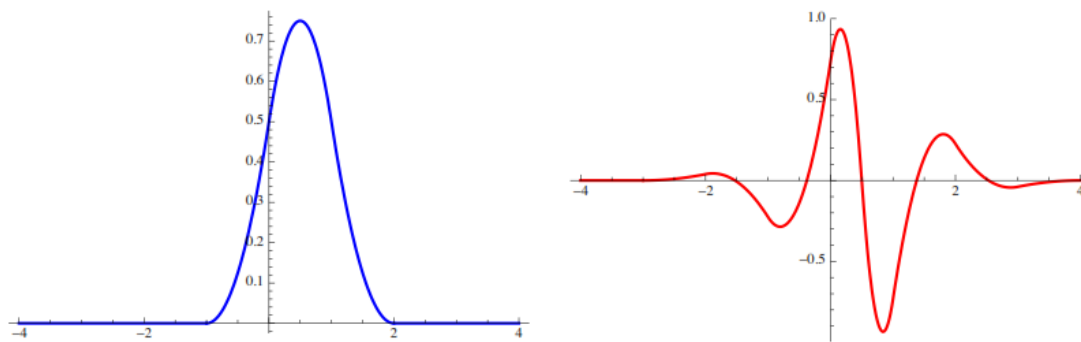
(a) *A biorthogonal father wavelet*   **(b)** *A biorthogonal mother wavelet*

Figure (2.16). *A biorthogonal synthesis wavelet family*

Spline wavelets have received special attention in recent years due to their attractive properties for function synthesis, rather than analysis [39] [40]. B-spline wavelets are the synthesis wavelets of a biorthogonal wavelet family, and their father wavelets are given directly by B-splines shifted such that they support starts at the origin. These wavelets are not orthogonal, but are symmetric, differentiable, compactly supported and have a closed form expression. B-spline wavelets provide good localisation in time and frequency, and tend towards Gabor functions as the order of the spline tends to infinity, which have optimal localisation in both time and frequency with respect to the uncertainty principle [41]. These wavelets are shown in Figure 2.17. Note that the zero[th] order B-spline father wavelet is a tile, or binary function
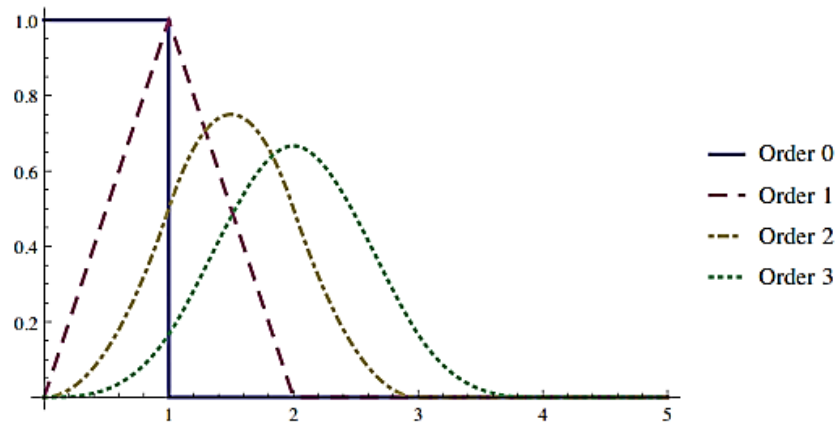
Figure (2.17). *B-spline wavelets of various orders*

Of all known wavelet types, B-splines will give the tightest approximation error bounds [42]. B-spline father wavelet functions are the smoothest possible father wavelets for a given compact support, and have the shortest support width for a given order. The B-spline father wavelet equation is given by repeated self-convolution of a tile across the unit interval [43]. Battle-Lemarie wavelets are orthogonal spline wavelets, although the spline is in the Fourier domain, meaning that the wavelet has good frequency localisation, but infinite support (although it has exponential decay). An example of this wavelet type is shown in Figure (2.18).
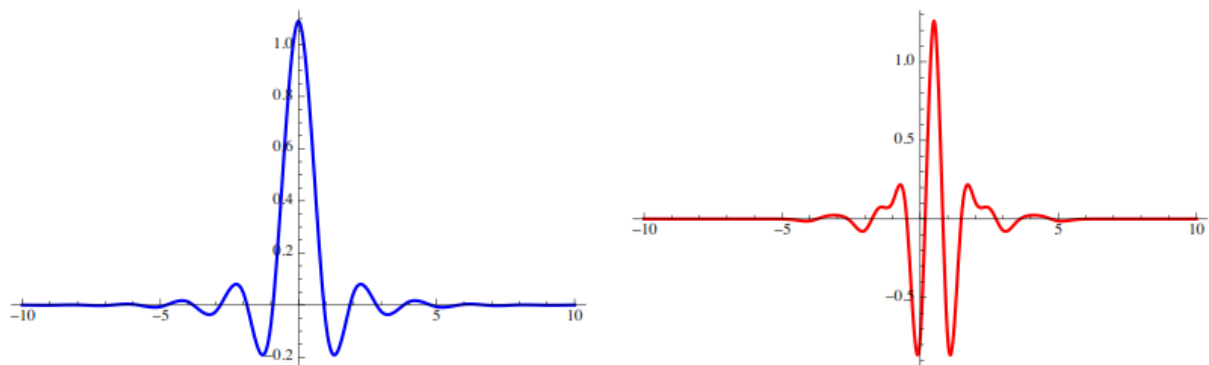
(a) *A Battle-Lemarie father wavelet wavelet*

(b) *A Battle-Lemarie mother*

Figure (2.18). *A Battle-Lemarie wavelet family*

However,The properties of these wavelet families are summarised in table 2.1 and table 2.2 .

Table 2.1**.** Comparative properties of wavelet families[44]

Family	Order	Support Width	Orthonormal	Symmetric
Haar	-	1	yes	yes
Daubechies	2n	2n-1	yes	no
Coiflet	2n	3n-1	yes	no
Symlet	2n	2n	yes	nearly
Shannon	-	R (Infinity)	yes	yes
Meyer	-	R (Infinity)	yes	yes
B-spline	n	n+1	no	yes
Battle-Lemarie	n	R (Infinity)	yes	yes

Table 2.2**.** Unique features of wavelet families [45]

Family	Special Properties
Haar	Best spatial localisation, worst frequency localisation
Daubechies	-Maximal vanishing moments for support width. - Robust, fast for identifying signals with both time and freq characteristics (use longer filters for better frequency resolution).
Coiflet	Additional vanishing moments in mother wavelets
Symlet	Least asymmetry in a compactly supported orthonormal wavelet
Shannon	Best frequency localisation, worst spatial localisation
B-spline	Tends towards optimal time-frequency localisation

2.9 Conclusion

In signal processing, wavelets have been widely investigated for use in filtering signals, among many other applications. A multiresolution analysis (MRA) is the design method of most of the practically relevant discrete wavelet transforms (DWT) and the justification for the algorithm of the fast wavelet transform (FWT) .the wavelet theory is then much complicated and is built up on theory of Riesz's bases. Moreover, the wavelet synthesis is not perfect anymore, since there is always an error between original and reconstructed signal

Chapter 3

The Usefulness of Wavelet

Transform to Reduce Noise in the

PCG Signal

3.1 Introduction

One of the major problems with PCG is noise corruption. Many sources of noise may pollute a PCG signal including lung and breath sounds, environmental noise and blood flow noises which are known as murmurs. These murmurs contain much information on heart hemodynamic which can be used, particularly in detecting of heart valve diseases. An automated system for heart murmurs processing can be an important tool in diagnostic of heart diseases using a simple electronic stethoscope. However, the first step before developing any automated system is the segmentation of the PCG signals from which the murmurs can be separated. A robust segmentation algorithm must have a robust denoising technique, where, wavelet transform (WT) is among the ones which exhibits very high satisfactory results in such situations. However, the selection of decomposition level and the mother wavelet are the major challenges. This work proposes a novel approach for an automatic selection of mother wavelet and level of decomposition that can be used in heart sounds denoising

3.2 Brief Overview of Discrete wavelet transform (DWT) denoising

The basic idea of DWT for one-dimensional signals is that the signal is split into two parts: a high-frequency component and low-frequency component. This splitting process is called signal decomposition. The edge components of the signal are largely confined to the high-frequency part. The signal is passed through a series of high-pass filters to analyze the high frequency components and low-pass filters to analyze the low-frequency components. Filters with different cutoff frequencies are used to analyze the signal at different resolutions. However, in the current study only orthogonal wavelets" Daubechies and Symlet" are examined since they allow perfect reconstruction of a signal. In Matlab environment, the Daubechies family of wavelets consists of 45 wavelets, and the Symlet family consists of 45 wavelets.

3.3 Noise in Wavelet Domain

Noise in DWT is considered as a source of information, especially for identifying systematic noise which is usually occurs at a specific location with low magnitude. When using wavelet for the denoised PCGs, the performance of our algorithm will be tested by adding noise to PCG signal. An empirically, noisy signal that is corrupted by additive noise which can be represented by the equation (2)

$$S_N(n) = s(n) + v(n), \quad n = 1,2,3 \dots \dots N \tag{3.1}$$

Where $s(n)$ is actual signal and $S_N(n)$ signal is corrupted by noise $v(n)$.

In denoising operation, the objective of noise removal is to reconstruct the original signal $s(n)$ from a finite set of $S_N(n)$ values without assuming a particular structure for the signal. So that it is important to monitor the influence of noise on our results and this requires simulation is run in MATLAB. Note that noise length $v(n)$ takes approximately the same actual signal length $s(n)$

3.4 Wavelet denoising

Figure 3.1 shows a general DWT denoising procedure with three main steps: (i) decomposition, (ii) thresholding detail coefficients and (iii) reconstruction. In the first step, signal is decomposed into several levels of approximation and detail coefficients. Decisions have to be made about an appropriate DWT method, a mother wavelet and number of de-composition levels (N). Denoising process rejects noise by thresholding in the wavelet domain, which is the second step. For thresholding detail coefficients one must decide about thresholding method and thresholding mode. The choice eventually involves a trade-off between keeping a bit of noise in the data and removing a bit of actual signal details. Finally, the denoised signal is reconstructed using approximation coefficients of the last level (N) and thresholded detail coefficients of all levels (1 - N).
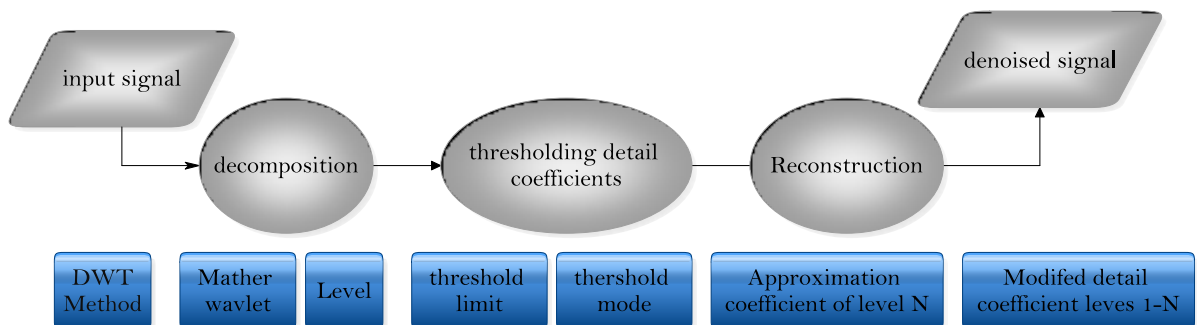
Figure (3.1). *General DWT denoising procedure, where thershold mode is soft or hard thresholding*

A more detailed and comprehensive explanation of DWT can be found in numerous publications, e.g. (Daubechies, 1992; Fugal, 2009). The thresholding process with its variants, threshold methods and threshold modes, is also presented

3.5 Threshold selection rules

Donoho and *Johnstone* gives a better understanding of how wavelet transforms work, and this understanding combined with nonlinear processing solves currently problems and gives the potential of formulating and solving completely problems. The method is based on tak-

ing the discrete wavelet transform (DWT) of a signal, passing this transform through a threshold, which removes the coefficients below a certain value. Generally, most of research work has used the universal threshold selection rule proposed by *Donoho*. Where, modified universal rules have been proposed as described in table 3.1

Table 3.1. Threshold selection rules

Thresholding rule	Description
Universal	It uses a fixed form threshold (Donoho &Johnstone, 1994) [47] which can be defined as $\beta = \sigma\sqrt{2log(N)}$, where N is the length in samples of time domain signal and σ is standard deviation of noise. The parameter σ can be estimated using median parameter which can be calculated as $\sigma = meadain\ (|cD_J|)\ /\ 0.6745$, where cD_J is the detail wavelet coefficients at scale level j and 0.6475 is a normalization factor.
SURE	Rigorous sure or shrink sure, it is used for One-Dimensional (1D) data, threshold achieved by minimizing Stein's Unbiased Risk Estimate depends on shrinkage function and the multi-resolution level. The sorted squared coefficients are computed as $S_c = \left(sort(|c|)\right)^2$, Then the threshold value is selected using the square root of the minimum risk as: $\beta = \sqrt{min\left(\frac{(N-2A)+(\sum_1^N S_{ci})+(B*S_c)}{N}\right)}$ where N=length(c) A=12..N and B=N-1,N-2,..0
Hybrid	This option attempts to overcome limitation of SURE. It is a mixture of the universal and the SURE rules. The exact conditions of this algorithm are described in Donoho and Johnstone (1995) [49].
Minimax	It uses a fixed threshold chosen to yield minimax performance for MSE against an ideal procedure. The minimax estimator is the option that realizes the minimum, over a given set of functions of the maximum MSE $$\beta = 0.3936\ +\ 0.1829\ \frac{log(N)}{log(2)}$$
Length Modified Universal rule (LMU)	It was modified by *Donoho* to be used with soft thresholding Function (*Donoho*, 1995)[50]. It is defined as $\beta = \frac{\sigma\sqrt{2log(N)}}{\sqrt{\bar{N}}}$

Scale Modified Universal rule (SMU)	It was modified by Donoho1992 [51] to be used with the level dependent method . It can be expressed as $\beta = \sigma\sqrt{2log(N)}.2^{\frac{j-1}{2}}$
Global Scale Modified Universal rule (GSMU)	It was modified by Zhong and Cherkassky (2000) [52] It is given by $\beta = \sigma\sqrt{2log(N)}.2^{-\frac{j}{2}}$
Scale Length Modified Universal rule (SLMU)	It is a combination between LMU and SMU rules by Donoho (1992)[51]. It is shown as $\beta = \frac{2\sigma\sqrt{2log(N)}}{2^{\frac{j-1}{2}}\sqrt{N}}$
Log Scale Modified Universal rule (LSMU)	It takes the different thresholds at different scales by Song and Zhao (2001) [53]. It can be defined as $\beta = \frac{\sigma\sqrt{2log(N)}}{log(j+1)}$
Log Variable Modified Universal rule (LVMU)	It was modified by Zhang and Luo (2006). The equation can be defined as $\beta = \frac{\sigma\sqrt{2log(N)}}{log[e+(j-1)^d]}$, experiment of *Zhang* and *Luo* (2006) [54] showed that the constant d is associated to the wavelet function where d should be ranging between 0 and *3*

3.5.1 Threshold rescaling methods

All threshold selection rules can be smoothing their thresholds by using rescaling methods. In threshold rescaling, three categories can be identified: global (GL), first-level (FL) and level dependent (LD) (*Elena et al.*, 2006; *Johnstone* & *Silverman*, 1997) [55, 56]. In the first one, standard deviation of noise (σ) can be adapted to three categories (GL, FL and LD). While the second one, length of wavelet coefficients (N) can be adapted to only GL and LD thresholding. To identify the threshold rescaling methods, GL defines σ as the estimated standard deviation of all wavelet coefficients and N as the length of the total wavelet coefficients. FL defines σ_1 as the estimated standard deviation of the first-level detail coefficients (cD_1). LD defines σ_j as the estimated standard deviation for every possible decomposition levels and N_j as the length of the wavelet coefficients at decomposition level j.

3.6 Wavelet Threshold Function

3.6.1 Classical Threshold Function

The hard threshold function sets the decomposition coefficient to zero which is less than the threshold value under different scale spaces and reserves the decomposition coefficient which is greater than the threshold at the same time [47]. This method does not change the local properties of the signal, but because of the discontinuity, it leads to a certain fluctuation in the reconstruction of the original signal. It is defined as

$$c\widetilde{D}_j = \begin{cases} 0, & |cD_j| < \beta_j \\ cD_j, & |cD_j| \geq \beta_j \end{cases} \tag{3.2}$$

The soft threshold function is to select the specified threshold value of the decomposition coefficient to zero. After the algorithm, the decomposition coefficient is coherent, but it loses a part of the high frequency coefficients above the threshold (Donoho & Johnstone, 1994) [47].The soft threshold function is determined by:

$$c\widetilde{D}_j = \left\{ \mathrm{sign}(cD_j)(|cD_j| - \beta_j), \ |cD_j| \geq \beta_j \right. \tag{3.3}$$

Where cD_j and $c\widetilde{D}_j$ are noisy and denoised wavelet coefcients, respectively, at the jth decomposition level.

3.6 .2 The Improved Threshold Function

The continuity in the soft threshold function is much better, but it has a constant deviation. So, in order to overcome its shortcomings.   Modified soft threshold function have been proposed In this chapter. where we provide the specific name to each function as follows.

Threshold Function	Description
Mid function (MID)	It is an extension of soft threshold Function (Percival & Walden, 2000) [57], small wavelet's coefficients are zeroed, and then large wavelet's coefficients are not affected. intermediate wavelet's coefficients are reduced by $$c\widetilde{D}_j = \begin{cases} cD_j & |cD_j| \geq \beta_j \\ 2\mathrm{sign}(cD_j)(|cD_j| - \beta_j), & |cD_j| \geq \beta_j \\ 0 \ otherwise \end{cases}$$
Hyperbolic function (HYP)	It is described in Vidakovic (1999) [58] work and its equation is defined same as modulus squared function (Guoxiang & Ruizhen, 2001) [59]that is given by

	$c\widetilde{D}_j = \left\{ \text{sign}(cD_j)\sqrt{(cD_j{}^2 - \beta^2)}, \quad \|cD_j\| \geq \beta_j \right.$
Modified hyperbolic function (MHP)	It combines the advantage of hard and soft functions. It is modified by *Poornachandra et al.* (2005) [60] and is shown as $$c\widetilde{D}_j = \left\{ \begin{matrix} (k.cD_j) \\ 0, \quad otherwise \end{matrix} \left[1 + \left(\frac{cD_j{}^2}{6} \right) \right], if \|cD_j\| > \beta_j \right.$$ where *k* is the scaling function and, in studies using 1 for the constant *k*.
Non-negative Garrote function (NNG)	It combines *Donoho* and *Johnstone*'s thresholding function with *Breiman*'s *NNG*. The equation is modified by *Gao* (1998) [61] as $$c\widetilde{D}_j = \left\{ \begin{matrix} cD_j - \dfrac{\beta_j^2}{cD_j} , f \|cD_j\| > \beta_j \\ 0, \quad otherwise \end{matrix} \right.$$
Compromising of hard and soft function (CHS)	It estimates wavelet's coefficients by weighted average of hard and soft (*Guoxiang* & *Ruizhen*, 2001) [62] . It can be expressed by $c\widetilde{D}_j = \left\{ \text{sing}(cD_j)(\|cD_j\| - \alpha\beta_j), \quad \|cD_j\| \geq \beta_j \right.$ Where For $0<a<1$, when α is 0, it changed into HAD and when α is 1, it changed into SOF
Weighted Averaging function (WAV)	It estimates coefficients by weighted average of HYP and hard (Zhang & Luo, 2006) [54]. It is given by $c\widetilde{D}_j = \left\{ (1 - \alpha)\text{sing}(cD_j)\sqrt{(cD_j{}^2 - \beta_j^2)} + \alpha(cD_j), if \|cD_j\| \geq \beta_j \right.$ where $0 < \alpha < 1$. If α is 0, will change to HYP and it will change to hard, if α is 1.
Adaptive Denoising function (ADP)	It is modified based on soft (*Tianshu et al.*, 2002) [63]. It is given by $c\widetilde{D}_j = cD_j - \beta_j + \dfrac{2\beta_j}{1 + e^{2.1cD_j/\beta_j}}$
Improved function (IMP)	It is attempted to address the deficiency of HAD and SOF (*Su* & *Zhao*, 2005) [64]. It can be defined as $c\widetilde{D}_j = \left\{ \text{sing}(cD_j)\left(\|cD_j\| - k^{(\beta_j - \|cD_j\|)}.\beta_j\right), \quad \|cD_j\| \geq \beta_j \right.$ Where $k \in R^+ \text{ and } k > 1$.

3.7 Comparison assessments by denoising application

The most reasonable way to test the effect of noise on a signal is determining the effectiveness of the algorithm through the comparison between the original signal and denoised signal. Many methods have been proposed to measure the effectiveness of denoising algorithms. In this respect, the signal to noise ratio (SNR) , estimation of mean square error (MSE) and Factor of distortion are carried out in measuring the effectiveness of the algorithm against noise densities of the PCG signal. In optimal SNR, higher SNR value indicates high performance results, while low SNR value indicates low performance resulting. Whereas in minimum error, denoised PCG signal have minimum mean square error (MSE) with the original PCG signal. In this study, the most important factors determining the SNR level are the decomposition level and the filter order of DWT. Mathematical expressions of SNR , MSE and Factor of distortion are given by the equation (3.4) , (3.5) and (3.6) [65] [66]

$$SNR = 10log_{10}\frac{Var(PCG)}{Var(PCG - PCG')} \tag{3.4}$$

And

$$MSE = \frac{\sum_{i=1}^{n}(PCG - PCG')^2}{n} \tag{3.5}$$

$$Ks = 10log\left(\frac{\left[\sum_{n=0}^{N-1} PCG - PCG'\right]^2}{\sum_{n=0}^{N-1} PCG^2}\right) \tag{3.6}$$

Where, Var is the variance operator, PCG' is the synthesis signal (signal after filtering), PCG is the original signal and *n* denotes the length of the signal

3.8 The proposed approach for selecting DL and order

In this section, we proposed a new approach to selecting optimal DL and the best mother wavelet for PCG signal, which are more appropriate for real time denoising operation. The results of this study will be between Symlet and Daubechies wavelet family under simulative noise added to the clean signal. The proposed approach is organized in (2) sections as follows: Section (1) explains the procedure used to compute the SNR (i, j) matrix, the highest value of SNR is chosen as a principal parameter in selection of mother wavelet and level of decomposition (DL) that can be used in heart sounds denoising. Where the rows of SNR matrix corresponds to the names of the wavelet and the columns correspond to DL.

Section (2) explains the second method for computing optimal wavelet (or order) and optimal DL under several maximum values of SNR.

3.8.1 Section (1)

In this Section, the analytic steps of proposed algorithm are based on matrix SNR which has a unique maximum value as follows:

1- Firstly, read the $PCG = \{PCG(n)\}_{n \in z}$ signal from a wave file (*.wav) where n corresponds to the number of signal coefficients.

2-Normalize the noisy PCG signal by equation (3.7)

$$PCG_{norm}(n) = \frac{PCG(n)}{\max(|PCG(n)|)} \tag{3.7}$$

3-Calculate the *maximum* decomposition levels (DL).and the *maximum* decomposition orders (DO) by equation (3.8)

$$\begin{cases} DLmax = log_2(N) \\ DOmax = log_2(N) \end{cases} \tag{3.8}$$

N is the length of discrete sampling signals.

4- For $1 \le i \le$ max (DO) and $1 \le j \le$ max (DL), Calculate the matrix SNRs (i, j) and matrix SNRd (i, j) are constructed by using Symlet and Daubechies wavelet family respectively as shown in Figure (3.2).

5-Calculate the maximum value of SNRs and SNRd.

6- Select optimal order and the optimal DL by finding row and column of the maximum value of SNRs and the maximum SNRd value.
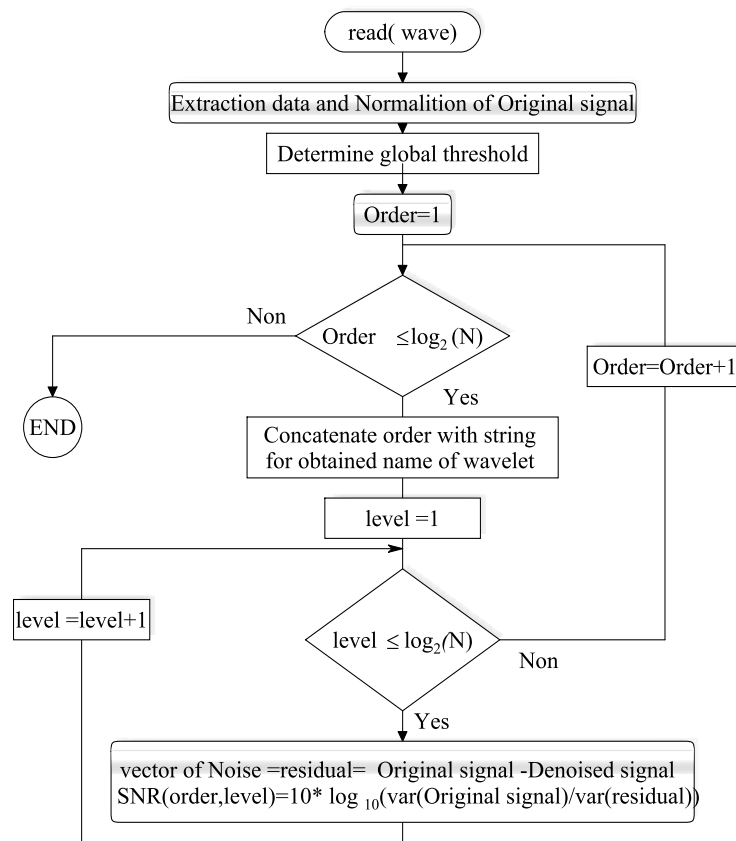
Figure (3.2). *flowchart represented a method of computing SNR(order,level) matrix under different orders(DO) and decomposition levels (DL)*

3.8.2 Section (2)

The analytic steps proposed in this section are based on SNR matrix has several maximum values. In this context, we propose method providing simultaneously the optimal wavelet with the optimal DL by using the following steps:

Step 1: Find row (wavelet name) and column (level) at each maximum SNR value as shown in Figure (3.3).

Step 2: From step (1), find all signals to different wavelet names and DL of max SNR value.

Step 3: Calculate error MSE from the equation (3.5) at each signal.

Step 4: Choose the denoised signal according to less error value.

Step 5: Determination the row and the column related to the selected signal denoising.

Step 6: From step (5), select optimal order and optimal DL.
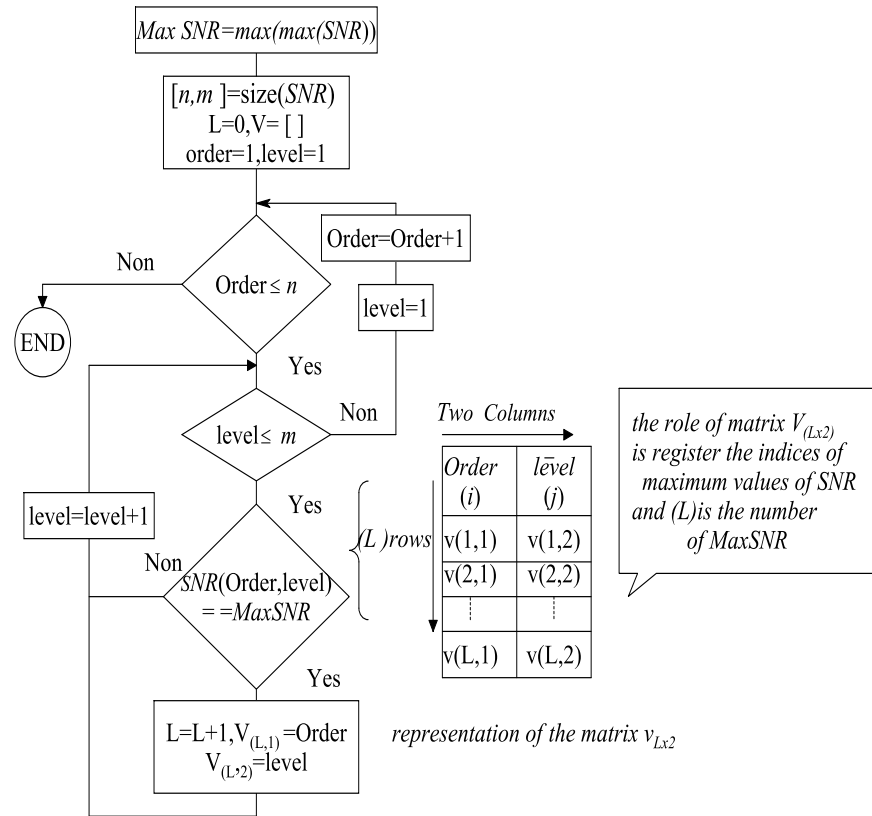
Figure (3.3). *flow chart for the computing numbre of the maximum value of SNR matrix*

3.9 Efficiency Criteria

In this chapter, different tests are carried out to evaluate the proposed algorithm in addition to the issues of the choice of wavelet families for PCG signal denoising, where the current methods do not focus mainly on the choice of DWT that is necessary to separate noise, because that these methods are mostly applied in image processing applications which use specified wavelets. However, experiment method to select the appropriate wavelet can be challenging in finding an appropriate wavelet. The evaluation of the algorithm is based mainly on coherence analysis and also on denoising quality under varying the DL and optimal wavelet. The retention of signal structure is important and SNR cannot differentiate between distorting and non-distorting noise in the signal, and hence SNR do not provide an accurate measure of quality. Initially, the evaluation of the algorithm is carried out by calculating the correlation coefficient. It is important to note that it can't be used for phase difference of signals, but generally it gives important information in amplitude.

3.9.1 Correlation coefficient (**Corr**)

It is a measure that determines the degree quality between original PCG signal and denoised signal obtained under selected optimal mother wavelet and varying DL. Note that the changing of mother wavelet has influence on denoising quality. The better the correlation coefficient is near to one (Corr > 0, 95), while in case less than 0.90 indicates that signal denoising is poor. It is given by the equation (3.9)

$$corr.coef(DL) = \frac{cov\left(PCG_{(original)}, PCG_{(denoised)}\right)}{Var_{PCG_{(original)}} Var_{PCG_{(denoised)}}} \qquad (3.9)$$

Where *cov* is covariance.

3.9.2 Coherence (coh)

Coherence is computed between two signals clean and denoised provides a quantitative measure of denoising performance in the frequency domain [67]. Greater denoising performance results in higher coherence values, it is given by the equation (3.10)

$$Coh = \frac{|S_N S(f)|^2}{S_N(f)S(f)} \qquad (3.10)$$

Where S_N *S* (*f*) is the cross-spectral density between S_N (*n*) and *S* (*n*), S_N (*f*) and *S* (*f*) their respective auto-spectra. The hamming window of data points is used for reducing the variance of the resulting spectral estimate with 50% overlap, while the values of coherence will always satisfy 0≤ *Coh* ≤ 1. However, coherence is a widely used measure for characterizing linear dependence between a pair of signals. For nonstationary signals, the autospectrum, cross spectrum, and coherence between signals may evolve over time. For stationary stochastic processes, coherence between two signals may vary across frequency but remains constant over time. That is, linear dependence between two stationary signals does not change with time

3.10 Conclusion

   Selection of suitable wavelet denoising parameters is important for the success of the PCG signal filtration in the wavelet domain, because there is currently no known method to calculate the combination of the wavelet denoising parameters that gives the best results. Therefore, many works have tried to find the optimal wavelet denoising parameters which lead to maximum filtration performance. In this regard, we propose method allow for us to find the optimal wavelet with the optimal level of decomposition simultaneously.

Chapter 4

Experimental Results and

Performance Evaluation

4.1 Introduction

Signal denoising remains to be one of the main problems in the field of signal processing. When using wavelet to denoise PCGs, there are many factors that must be considered. Examples of such factors are mother wavelet and level of decomposition. In order to obtain perfect reconstruction after signal decomposition, only orthogonal wavelets will be considered. In Matlab environment, Symlet family and the Daubechies family of wavelets are consists of 45 wavelets.

one of the major problems with PCG is noise corruption. Many sources of noise may pollute a PCG signal including lung and breath sounds, environmental noise and blood flow noises which are known as murmurs. Various tools and methodologies have been proposed for denoising of heart sound signals. Among all the surveyed methods for PCG signal denoising, the wavelet transform is the most widely used and efficient, because it can analyze signals at different resolutions using the various wavelet families available. This study focuses on denoising of phonocardiogram (PCG) signals using Symlet and Daubechies wavelet by the selected mother wavelet and decomposition level.Since denoised signals are compared with the original PCG signal to determine the most suitable parameters for the denoising process.

The PCG signal that used in the work is part of the cardiac auscultation of heart murmurs database which provided by E-General Medical Inc. Data set recorded from Phonocardiograph having 64 signals is available in [68], it is taken from clinical using the digital stethoscope and from the PASCAL database has 176 recordings for heart sound segmentation and 656 recordings for heart sound classification. Although the number of the recordings is relatively large, the recordings have the limited time length from 1s to 30s; it is available in [69]. The data include not only clean heart sounds but also very noisy recordings.

4.2 Experimental Procedure

The SNR and coefficient distortion Ks are carried out in measuring the effectiveness of the symlet wavelet against noise densities with time required for reconstruction of PCG signal as shown in below tables . the Systolic Pulmonary Stenosis (PS) signal is corrupted by random and White Gaussian noise .

Table 4.1 : Results for denoising PS signal by application of symlet wavelet

Wave-let	Level 5 decomposition with addition of 1.7750dB noise											
	Additive White Gaussian noise						Random noise					
	Soft thresholding			Hard thresholding			Soft thresholding			Hard thresholding		
	Time	Ks	SNR	Time	Ks	SNR	Time	Ks	SNR	Time	Ks	SNR
Sym1	0.05	43,8	3,57	0.05	41,5	3,81	0.05	6,7	13,2	0.05	5,91	12,27
Sym2	0.05	41,9	3,76	0.05	36,0	4,42	0.05	3,5	16,6	0.05	3,75	14,25
Sym4	0.05	31,9	4,96	0.05	28,1	5,51	0.05	3,6	16,3	0.05	3,03	15,18
Sym6	0.05	28,2	5,48	0.05	25,7	5,89	0.05	3,2	17,3	0.05	2,76	15,59
Sym8	0.06	27,5	5,59	0.05	25,7	5,89	0.05	3,2	18,6	0.05	2,63	15,78
Sym10	0.05	26,2	5,80	0.05	24,0	6,18	0.05	3,1	17,3	0.05	2,76	15,58
Sym12	0.05	24,3	6,12	0.05	23,9	6,21	0.05	3,1	18,6	0.05	2,51	15,99
Sym14	0.05	22,5	6,46	0.05	25,3	5,95	0.05	2,9	18,6	0.05	2,57	15,88
Sym16	0.05	22,8	6,44	0.05	24,3	6,13	0.05	2,9	18,7	0.05	2,57	15,89

From Table 4.1,sym14 and sym16 approximately gives the same performance in soft thresholding for AWGN. In case of hard thresholding, sym12 has high SNR value while Sym 1 has lower SNR (3,81 dB). In addition , almost all wavelets have the same time of reconstructing signal. A result in soft thresholding under using random noise, Maximum SNR is at sym16. while in the case of hard thresholding, Sym12 has the maximum SNR than others.
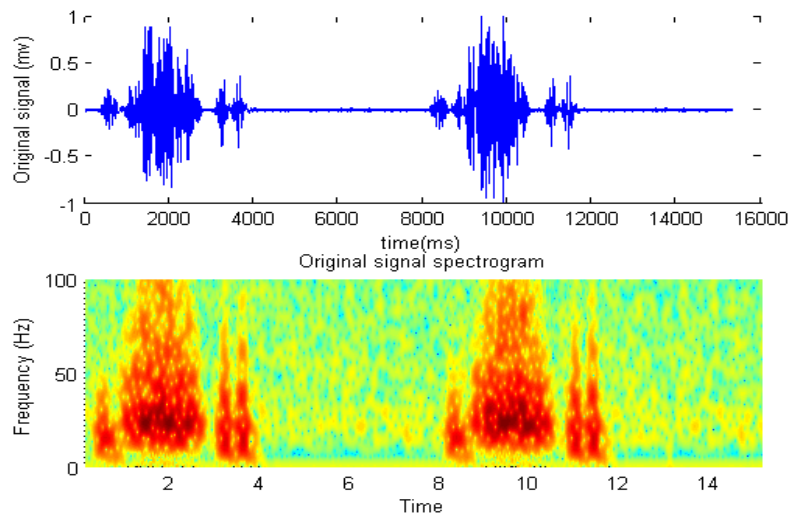
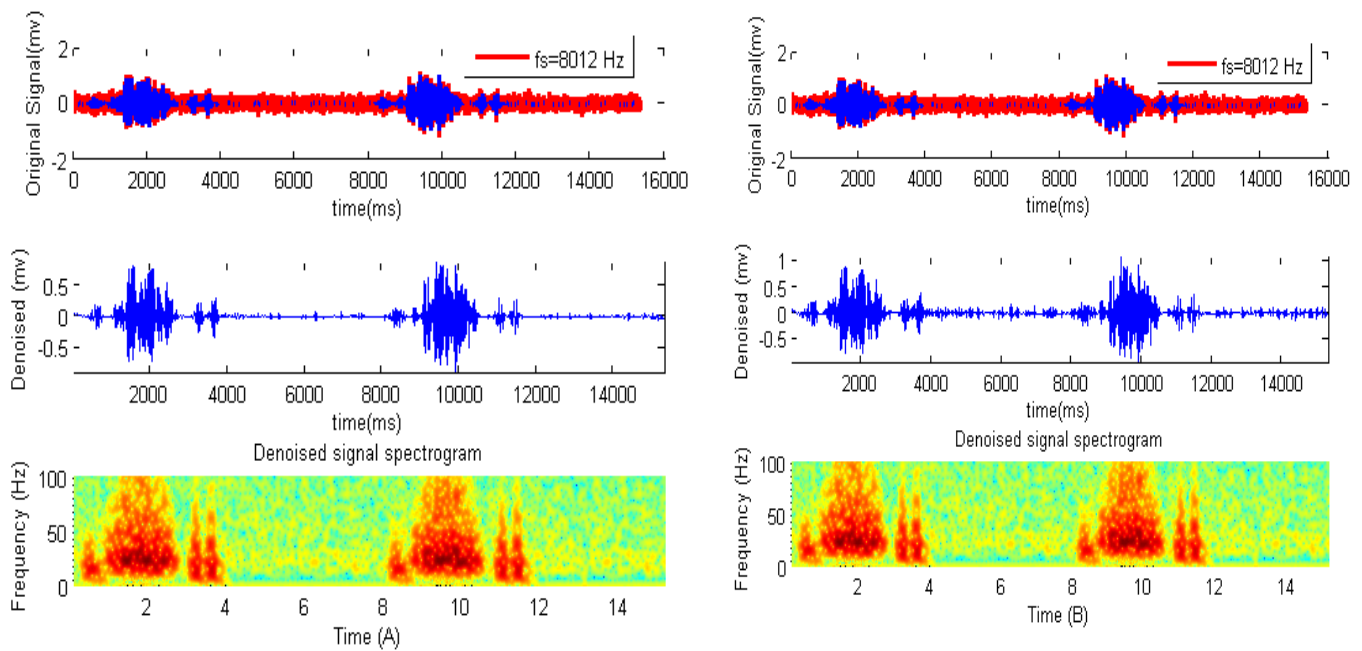**Figure** (4.1): *Original Signal and its Spectrogram*

Figure (4.2) *:the representation of the original and the denoised PS signal with its spectrogram using sym 16 and sym12 in case of soft and hard thresholding respectively*

Table 4.2: Results for PS signal by application of symlet wavelet

Level 5 decomposition with addition of 7.7956 dB noise											
Wavelet	Additive White Gaussian noise						Random noise					
	Soft thresholding			Hard thresholding			Soft thresholding			Hard thresholding		
	Time	Ks	SNR	Time	Ks	SNR	Time	Ks	SNR	Time	Ks	SNR
Sym1	0.043	18,05	7,43	0.037	17,21	7,64	0.036	2,5	15,87	0.03	2,39	16,20
Sym2	0.038	14,49	8,54	0.037	11,66	9,33	0.038	1,7	17,60	0.03	1,21	19,15
Sym4	0.038	21,12	9,63	0.037	8,57	10,66	0.039	1,1	19,46	0.03	1,01	19,93
Sym6	0.039	13,96	10,34	0.038	7,98	10,97	0.039	1,1	19,55	0.03	0,94	20,22
Sym8	0.040	10,24	10,52	0.038	8,12	10,90	0.039	1,1	19,40	0.039	0,92	20,32
Sym10	0.039	14,15	10,51	0.039	7,90	11,02	0.039	1,1	19,27	0.039	0,99	20,03
Sym12	0.039	17,33	7,94	0.039	12,22	9,12	0.039	1,1	19,45	0.039	0,98	20,06
Sym14	0.039	14,76	8,35	0.038	12,43	9,05	0.039	1,0	19,76	0.039	0,96	20,16
Sym16	0.039	14,15	8,53	0.039	11,85	9,26	0.039	1,0	19,85	0.039	0,96	20,14

From Table 4.2 , hard thresholding for AWGN, sym1, sym4 and sym2 takes lower time for reconstruction.while sym10, sym12 and sym16 have   the same   time for reconstruction. Sym10 has maximum SNR (11.02 dB) than others. in soft thresholding , Sym8 has the best SNR value but it takes more time. Sym1 gives high value of time for reconstruction. For random noise, 8 sym takes more time in hard thresholding and sym 16 is the better but takes more time. SNR is very less at sym1 as compared to others. sym1 takes lower time for reconstruction of signal . Sym16 has maximum SNR than others in thresholding function.
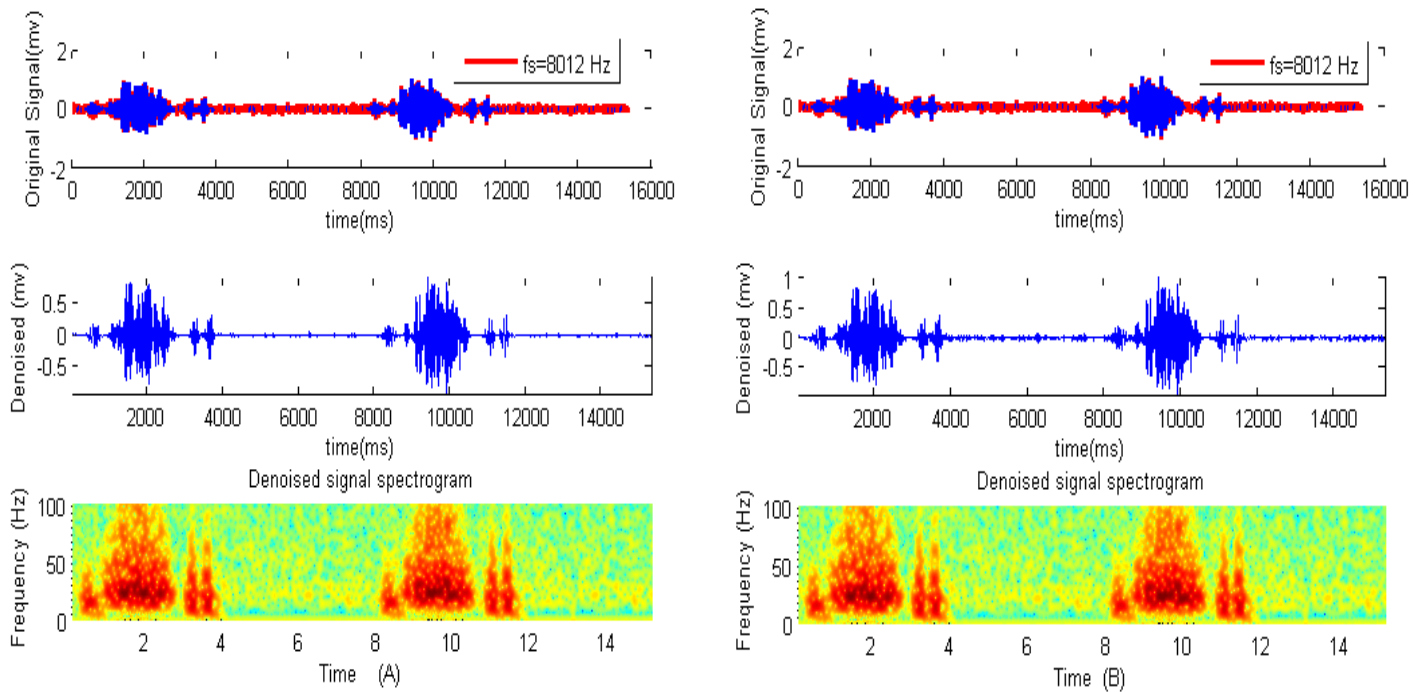
Figure (4.3) : *the representation of the original and the denoised period of PS signal with its spectrogram after denoising under using sym 16 and sym 8 and random noise in case of soft and hard thresholding respectively*

Table 4.3: Results for PS signal by application of symlet wavelet

Level 5 decomposition with addition of **15** dB noise											
Wavelet	Additive White Gaussian noise						Random noise				
	Soft thresholding			Hard thresholding			Soft thresholding			Hard thresholding		
	Time	Ks	SNR	Time	Ks	SNR	Time	Ks	SNR	Time	Ks	SNR
Sym1	0.036	41,14	3,85	0.036	33,11	4,799	0.036	2,3	16,30	0.072	2,26	16,44
Sym2	0.038	19,65	7,06	0.038	21,3	7,94	0.038	1,3	18,70	0.037	1,190	19,24
Sym4	0.039	16,67	7,78	0.038	15,35	8,13	0.038	0,9	20,25	0.038	0,89	20,45
Sym6	0.039	14,27	8,45	0.039	15,61	8,06	0.038	0,8	20,73	0.038	0,90	20,43
Sym8	0.039	22,97	6,38	0.045	16,03	7,94	0.039	1,1	19,30	0.042	0,96	20,14
Sym10	0.039	19,96	6,99	0.040	14,99	8,23	0.039	0,7	21,01	0.039	0,83	20,76
Sym12	0.039	17,53	7,56	0.040	15,17	8,18	0.038	1,2	19,14	0.039	0,90	20,43
Sym14	0.040	18,26	7,38	0.039	15,30	8,15	0.039	0,7	21,03	0.039	0,90	20,45
Sym16	0.041	13,65	8,64	0.039	15,24	8,16	0.039	1,1	19,49	0.041	0,87	20,57

From the results shown in Table 4.3, in hard thresholding results for AWGN of 15 dB, the Sym10 takes maximum SNR value than other wavelets. While soft thresholding, Sym16 gives highest SNR but takes more time for signal reconstruction. On the other hand , Sym1 wavelet has least SNR with lower reconstruction time for hard and soft thresholding. For

Random noise, Sym14 gives highest SNR in soft thresholding while sym 10 has maximum SNR value than other in hard thresholding.

.
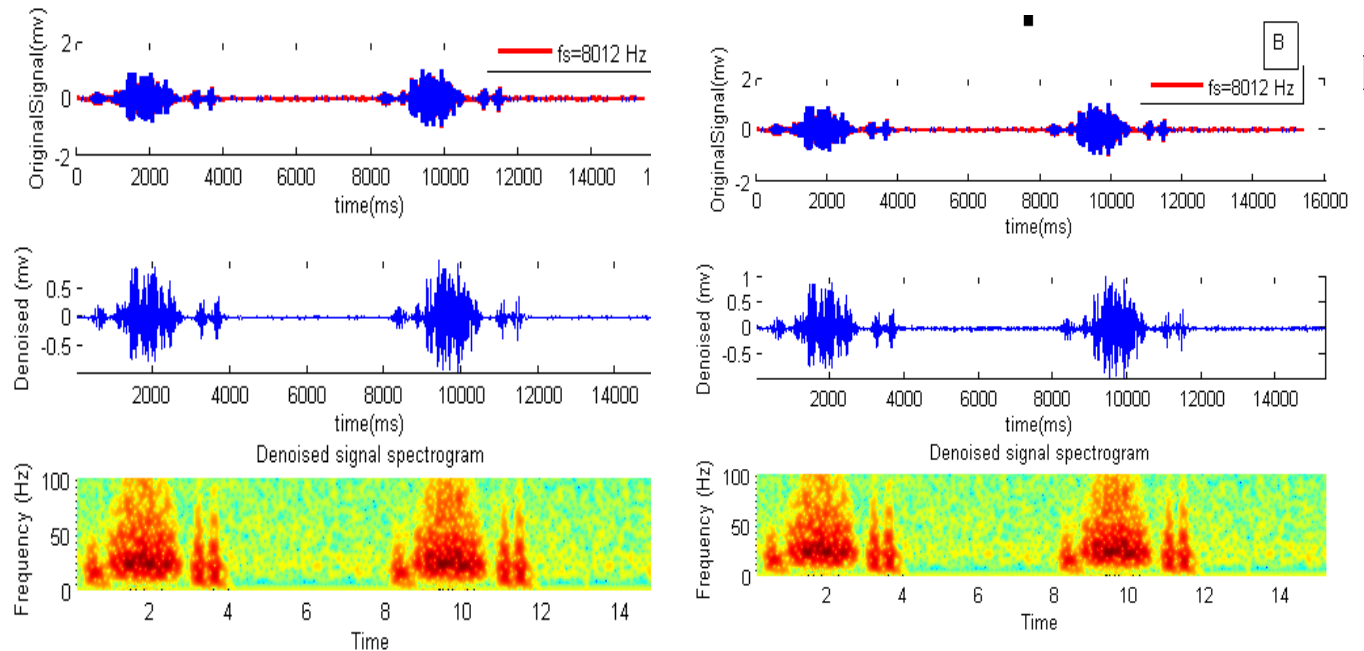
Figure (4.4) :*the presentation of the original and the denoised period of PS signal with its spectrogram under using sym 14 and sym10 and random noise in the case of soft and hard thresholding respectivly*

From figure (4.3) and (4.4) , it is observed that denoised signal is approximately identical to original signal when using sym 14 , sym 16 in case soft thresholding. In this study,Our algorithm provides two parameters, the mother wavelet and the level of decomposition. In this context; the different tests are carried out to evaluate our algorithm, all of Symlet and Daubechies wavelet families are used. The proposed algorithm is tested many times on data recorded from a wave file (*.wav) of different categories of patients. The results of the algorithm in Figure (4.5) is presented under simulation for four types of heart sound signals, which are corrupted by additive noise.

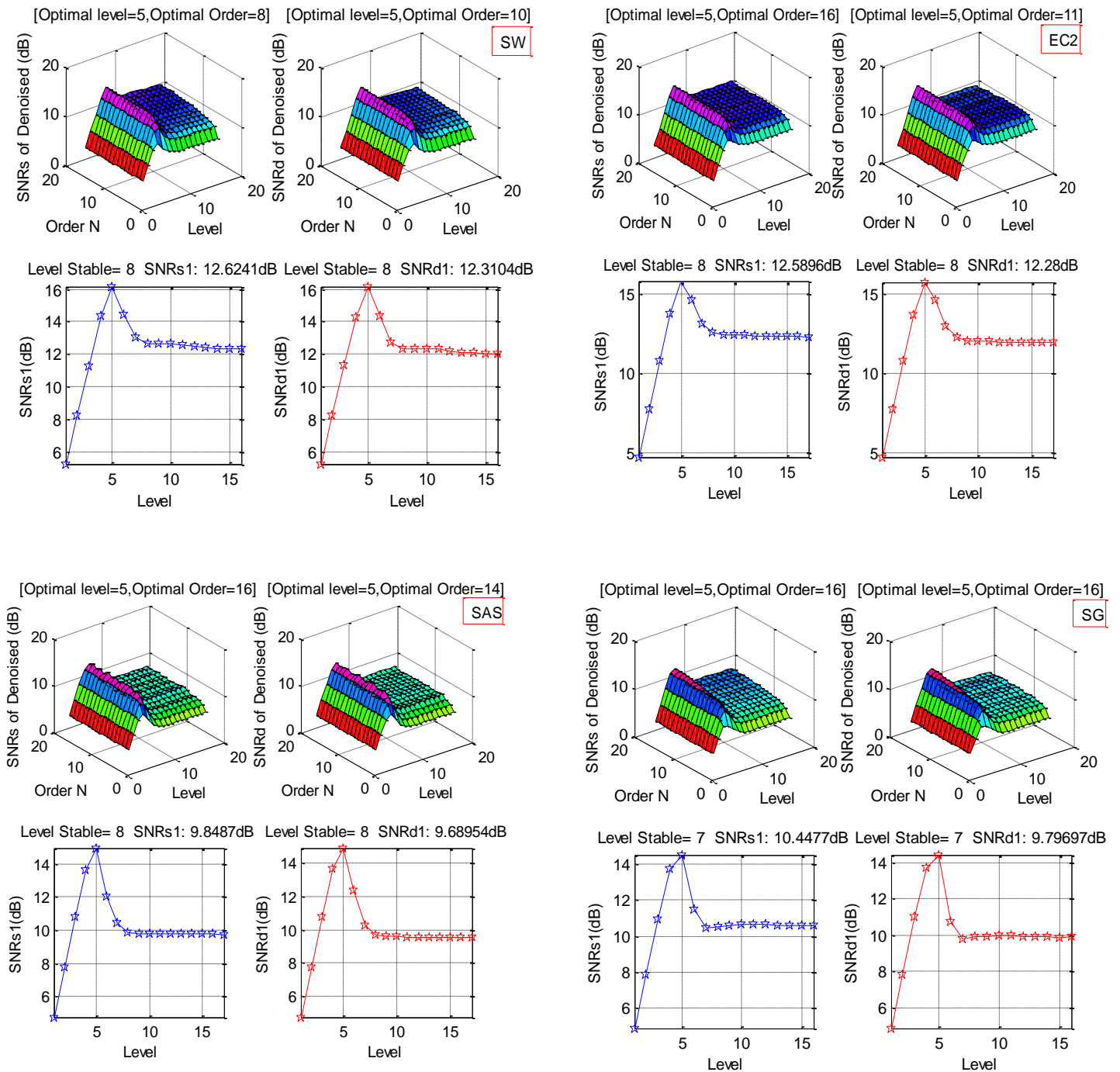**Figure** (4.5). *the comparison between SNRs and SNRd results under different parameter decomposition levels and Orders ,while SNRs1 and SNRd1 under varying decomposition levels and optimal order of wavelet through using Symlet and Daubechies wavelet to four PCG signals (SG, WS, SAS, SC2)*

Figure (4.5) shows that SNRs1 and SNRd1 vectors are increasing with the increased DL, then they become approximately stable once DL ≥ 7; this is due to the intensity of noise present in the detail components that has reduced through the increasing of decomposition level, because the amount of noise usually contains higher frequencies than low frequencies. While in DL ≥ 7, the influence of noise is very slight but statistical properties of the transformed signals are changed under varying levels of decomposition. Here, the successive DL loss progressively more high frequency information. It can be observed that the stability level of SNRs1 is slightly greater than the stability level of SNRd1. this implies that Symlet wavelet has shown superiority compared to Daubechies wavelet. The experimental results in a table (4.4) and (4.5) shown that the SNR values provide high denoising results, while MSE doesn't always give the most accurate estimate possible of signal denoising. In the other hand, we find that the number of maximum SNR matrix is always unique.

Table 4.4. comparison between Symlet and Daubechies wavelet for the selectivity of the order and the optimal DL under simulations of PCGsignals.

		SW signal Fs:22257 Hz	*SG* signal Fs:8000 Hz	SAS signal Fs:22050Hz	EC2signal Fs:22050Hz
maximum value threshold SNR	Max SNRd	16.1634	14.4265	14.8894	15.7454
	Max SNRs	16.1686	14.5268	14.9418	15.7524
Number of maximum SNRs values (L)		1	1	1	1
Number of maximum SNRd values (L)		1	1	1	1
Optimal level of Wavelet (*sym)*		5	5	5	5
Optimal order of Wavelet (*sym*)		8	15	16	16
Optimal level of Wavelet (*db)*		5	5	5	5
Optimal order of Wavelet (*db)*		10	16	14	11
frame length of signal (N)		79680	69421	221858	143312
Approximation max (DL) = $\log_2(N)$		16	16	18	17

Table 4.5. results obtained for the MSE, the SNR vector and coefficient correlation (Corr) by using the Symlet and Daubechies wavelet from 4PCG signals.

			SW signal Fs:22257 Hz	SG signal Fs:8000 Hz	SAS signal Fs:22050Hz	EC2 signal Fs:22050Hz
Saturated point	SNRs1 by Decibel (dB)		12.6241	10.4477	9.8487	12.9764
	Level (DL)		8	7	8	8
saturated point	SNRd1 by Decibel (dB)		12.3104	9.79697	9.68954	12.5896
	Level (DL)		8	7	8	7
MSEs			9.6072e^{-04}	9.6992e^{-04}	0.0025	7.4976e^{-04}
MSEd			9.6187e^{-04}	9.9257e^{-04}	0.0025	7.5098e^{-04}
Corr Coef (PCG, dPCG) (*sym*)			0.9881	0.9819	0.9838	0.9869
Corr Coef (PCG, dPCG) (*db*)			0.9881	0.9817	0.9838	0.9869

Note that MSEs and MSEd does not always related to perceived quality of reconstructed signals of wavelet

4.3 The evaluation of results by Correlation coefficient

According to table 4.5,The proposed method provides high denoising results (Corr> 0.98), since the best denoising is found through DL (5) as presented in Figure (4.6). Hence, the results are always situated in the maximum value of the SNR curve, which coincides perfectly with the highest correlation coefficient in most PCG signals. After level (5), there is a decrease in the correlation, but the results are always situated in high denoising part. The increasing of decomposition levels does not perturb the denoising quality after(DL≥7) because noise is extremely small and indistinguishable. In this test, the correlation coefficients are substantially low (Corr = 0.87) around level (1) and it provides a low denoising quality. In general, it can be observed that the increasing of decomposition level gives an increasing in denoising quality as presented in Figure (4.6), and the best denoising is found in the level (5).
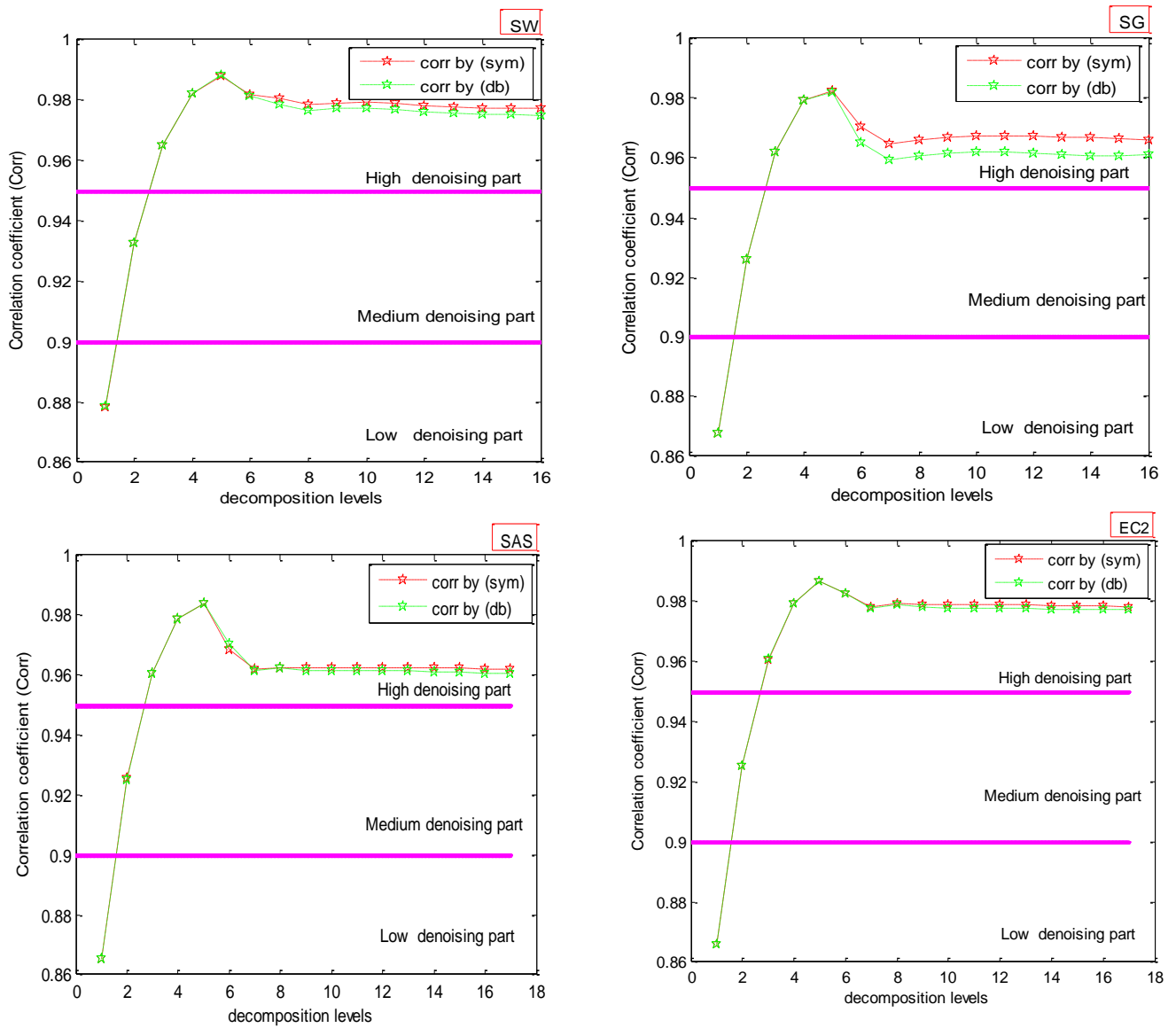
Figure (4.6). *presentation of moving correlation coefficient under different decomposition levels of Symlet and Daubechies wavelet for signals (SW, 22257 Hz), (SG, 8000Hz), (SAS, 22050H z) and (EC2, 22050 H z).*

It can be observed that the proposed algorithm preserves the main characteristic of the signal, and removes correctly the majority of noise by using Symlet wavelet as it is seen in Figure (4.7). The algorithm gives us the best results for retrieving the peaks of signals accurately that were submerged in the noise without distortion of the reconstructed signal.

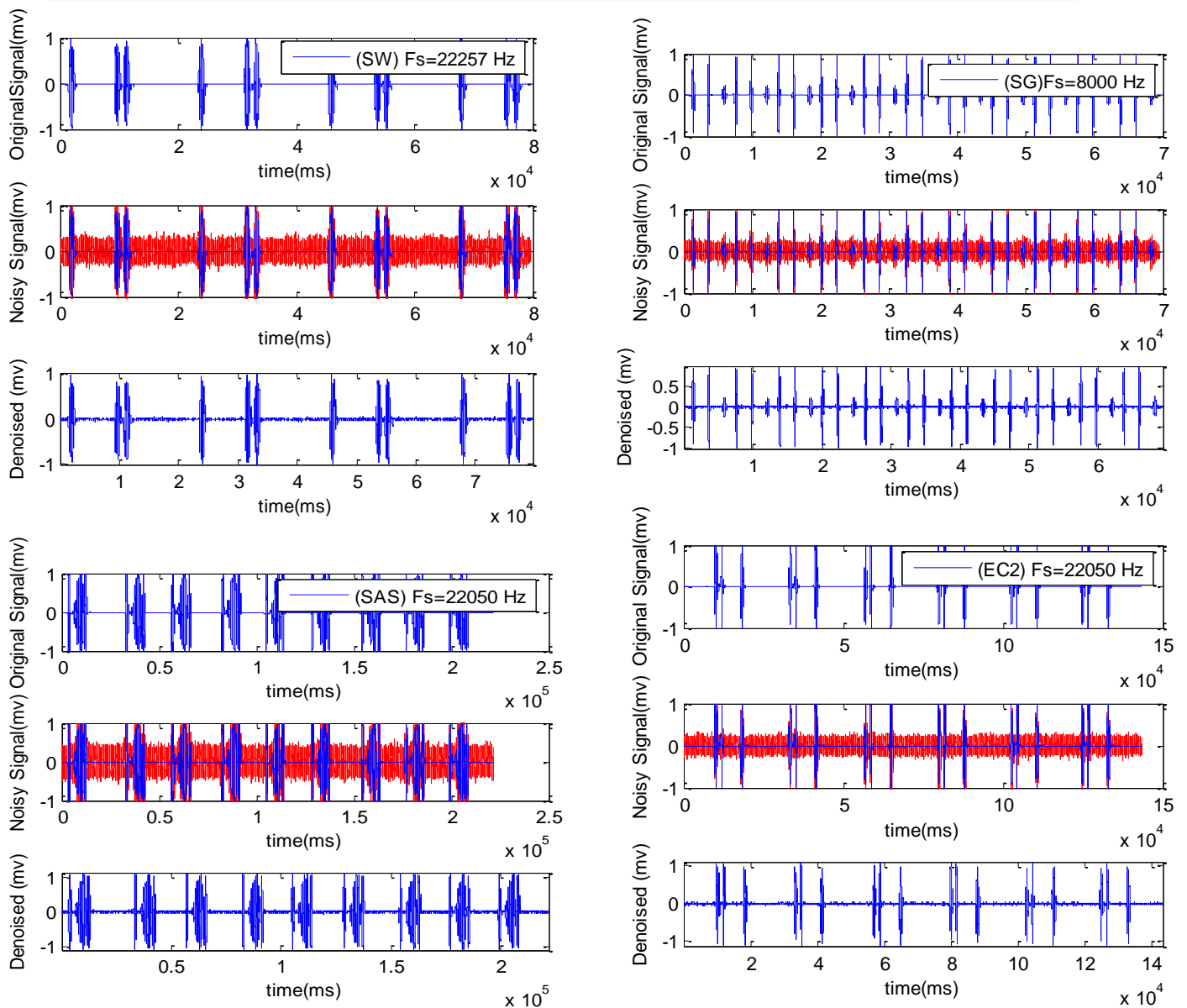**Figure** (4.7). *original signal, noisy signal and denoised signal for different pathological cases of PCG signals SW, SG, SAS, and EC2), where the signal amplitude is in arbitrary units (mv)*

4.4 The evaluation of results by coherence

From Figure (4.8) and (4.9), the performance of the wavelet is evaluated using coherence analysis under varying SNR and DL. In the most cases of PCG signals, very low DL (around 1, 2) gives in poor performance, since the coherence decreased dramatically and the reason behind that is initial DL like 1, 2 contain just noise; and hence the initial DL of wavelet can be used to eliminate a large part of noise. When DL takes a value (5), it achieves the highest SNR value with high coherence, and this means that the level (5) is an optimal value. Notably, when the DL is increased beyond 7, becames the SNR stable and the amount of coherence does not change. Here, we show that the influence of noise is constant and very

slight. Overall, results obtained in both qualitatively and quantitatively showed that the algorithm enables us to select the best level and the best mother wavelet.
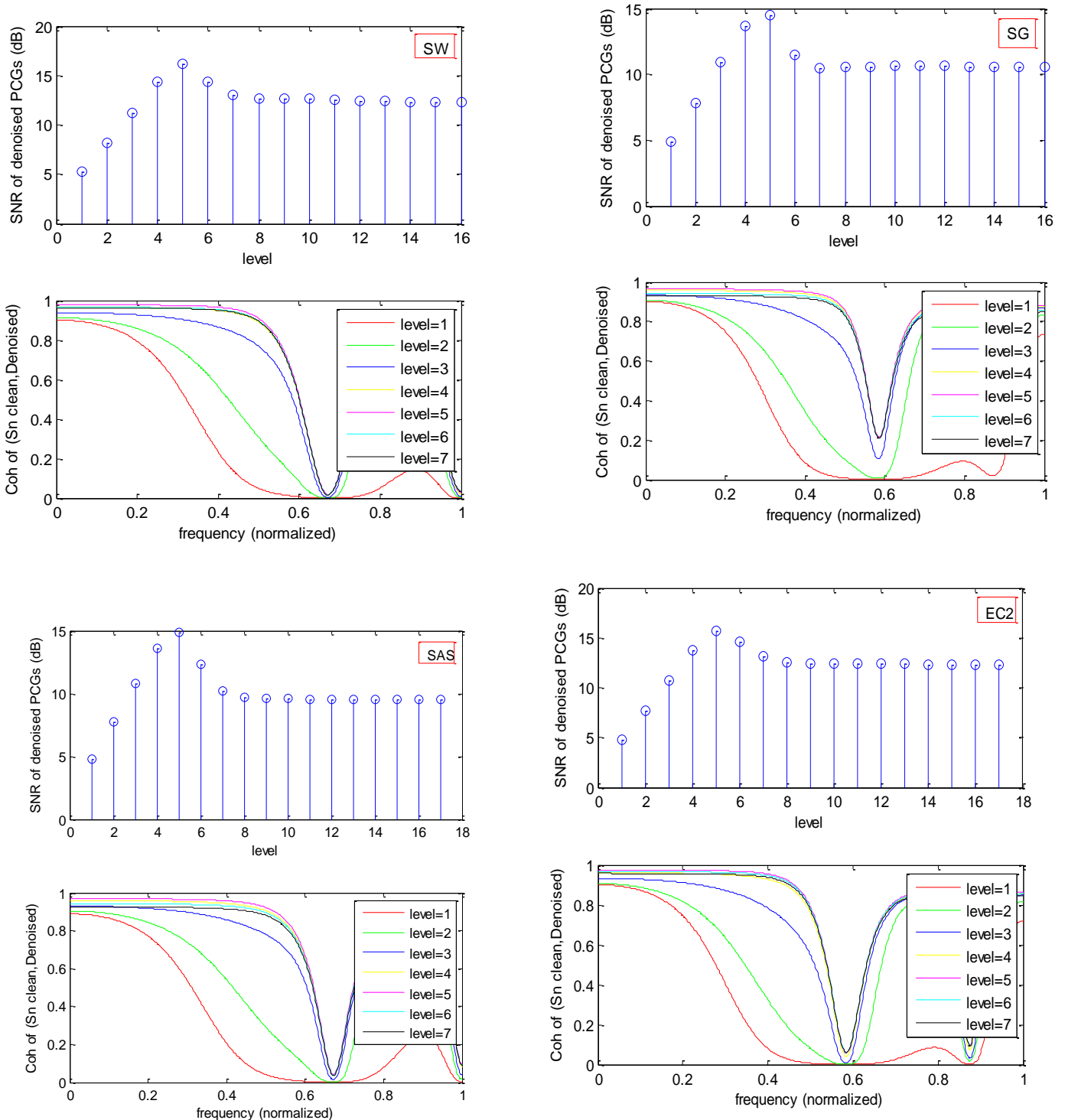

Figure (4.8). *presentation of SNR and coherence between the clean and denoised PCGs by using Symlet wavelet through different values of DL*
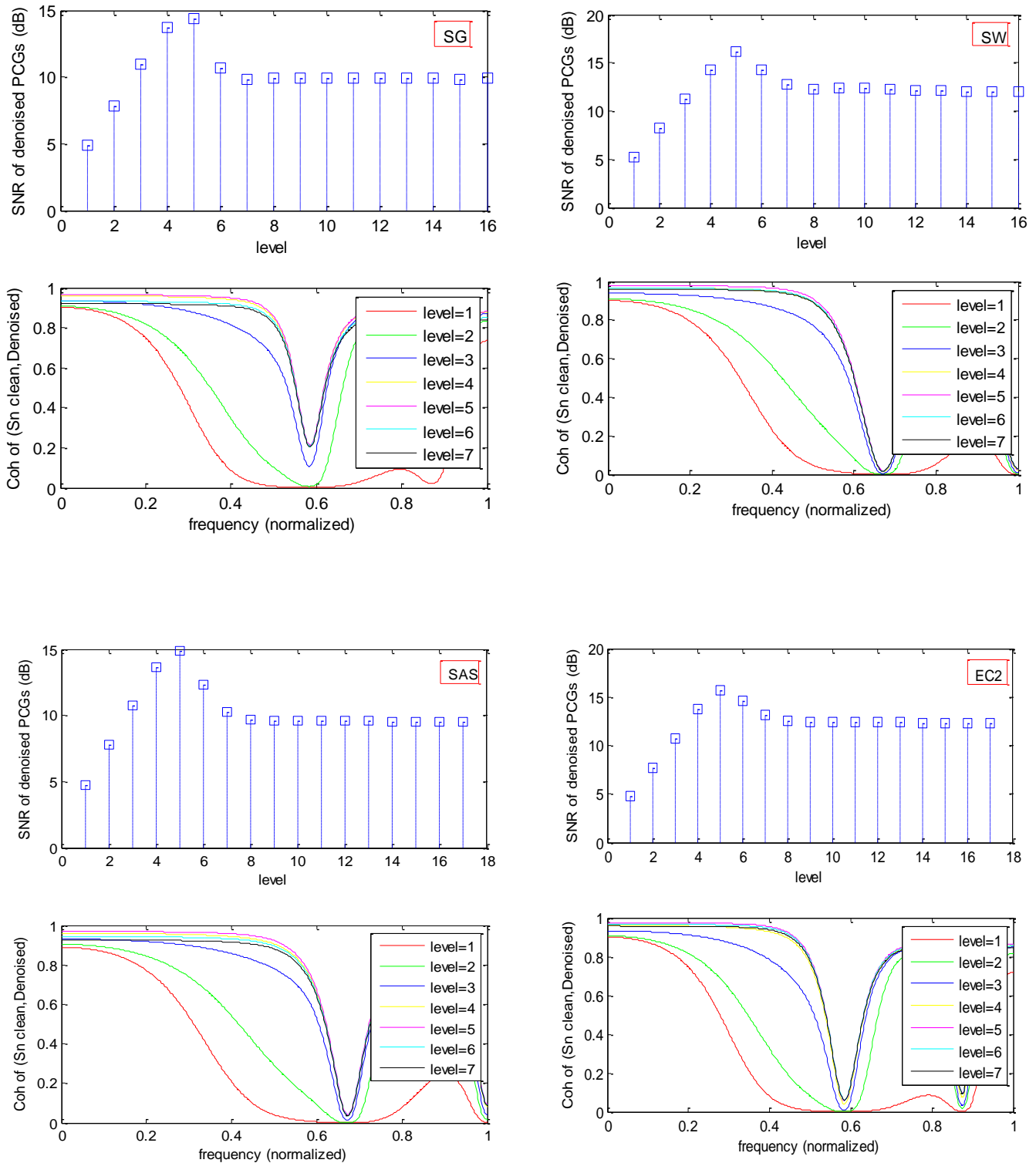
Figure (4.9). *presentation of SNR and coherence between the clean and denoised PCGs by using Daubechies wavelet through different values of DL*

Therefore, we can conclude that proposed method preserves the main characteristic of the signal with the highest SNR value when the decomposition level is five. This method is used for denoising of heart sound signals that are highly corrupted by noise, and the most important feature of the denoised signal obtained through our method is that it can be used for accurate diagnostics of cardiovascular diseases. Finally, Table (4.6) shows a comparison between our proposed algorithm results with the previous study results to see the efficiency of the proposed work.

Table 4.6. Comparison between our proposed algorithm results with the previously proposed results

Autheur	SNR (dB)	Correlation (Corr)	Mother wavelet	DL
Xiefeng Cheng and Zheng Zhang [70]	10.6385	0.9570	Db5	5
Tahar Omari [71]	-	0.973	db37	6
Abhishek et al. [72]	2.7233 and 2.723	-	Coif and Sym6	3 and 4
Abhishek et al. [73]	7.6556	-	Db2	4
Dawid and Redlarski [74]	13	-	Coif5	10
Mohammed Nabih Ali [75]	15.4307 and 15.6019	-	Discrete Meyer and Db10	4
Abhishek Misal and G. R. Sinha [76]	12.1663	-	Sym2	6
P.G. Student and Narendra B [77]	14.9138	-	db10	5
Feng et al. [78]	15.3	-	Coif wavelet family	8
Our proposed method	16.1634 and 16.1686	0.9881 0.9881	Db5 and sym8	5

4.5 Conclusion

In this work, we presented a new approach to determine the optimal decomposition level and the best mother wavelet in PCG denoising operation. The proposed method is based on the term SNR, which plays a crucial role in simulating the decomposition levels and orders of Daubechies and Symlet wavelet families. The optimal level and the optimal order can be determined by the maximum value of SNR matrix, which is always unique. In most PCG signals, we found that the maximum SNR coincides perfectly with the highest correlation coefficient and with the highest level of coherence. Furthermore, the proposed method can provide high precision and quality and giving us information that is not issued by other methods. According to the results, we see that Symlet wavelet gives slightly better results compared to Daubechies wavelet. Finally, we believe that our method is suitable for analyzing biomedical signal processing, and it can be realizable in real-time processing.

.

General Conclusion

General Conclusion

Noises are a main problem in the analysis of the PCG signal. Since, random noises that have their frequency components fall in the energy band of the PCG signal are the major problem. Wavelet is a theoretically powerful in denoising method, but its effectiveness is influenced by the issue of choosing of the decomposition level (DL) and order of filter when applied in various engineering applications. Hence, in this work, we presented a new approach to determine the optimal decomposition level and the best mother wavelet in PCG denoising operation. The proposed method is based on the term SNR, which plays a crucial role in simulating the decomposition levels and orders of Daubechies and Symlet wavelet families. The optimal level and the optimal order can be determined by the maximum value of SNR matrix, which is always unique. In most PCG signals, we found that the maximum SNR coincides perfectly with the highest correlation coefficient and the highest level of coherence. Furthermore, the proposed method can provide high quality and giving us information that is not issued by other methods. it is shown that our approach is able to effectively denoise and especially retrieve the signal peaks accurately. According to the results, we see that Symlet wavelet gives slightly better results from Daubechies wavelet. Finally, we believe that our method is suitable for analyzing biomedical signal processing, and it can be realizable in real-time processing. In future research, we intend to generalize our algorithm to determine the most suitable parameters for real-time signals. Also, we aim to develop a hardware implementation to perform the proposed algorithm.

Bibliographical references

Bibliographical references

[1] Alonso. F.: Detection of life threatening arrhythmias using feature selection and support vector machines. IEEE Transactions on Biomedical Engineering, Vol 61, No.3, pp.8328 40, (2014).

[2] Sang Y.F, Wang D, Wu JC (2010a) Entropy-based meth od of choosing the decomposition level in wavelet threshold de-noising. Entropy, ISSN 1099-4300

[3] Yan-Fang Sang, Dong Wang, Ji-Chun Wu, Ling Wang," The relation between periods' identification and noises in hydrologic series data" Journal of Hydrology. Volume 368, ISSN 0022-1694, pp.165–177, (2009)

[4] R. PRINCY, P. Denoising EEG Signal Using Wavelet Transform (IJARCET). Volume 4 Issue 3, ISSN: 2278 –1323, March (2015

[5] Y. H. Peng, "De-noising by modified soft-thresholding," in Proc. IEEE Asia-Pacific Conf. Circuits and Systems, pp. 760–762, (2000).

[6] L. Durand and P. Pibarot, "Digital signal processing of the Phonocardiogram: Review of the most recent advancements," *Critical Reviews in Biomedical Engineering*, vol. 23, no. 3-4, p. 163, 1995.

[7] L. Durand and R. Guardo, "A model of the heart-thorax acoustic system," *Applications of computers in medicine*, pp. 29–41, 1982.

[8] Williams, P. L., and Warwick, R. (1989). *Gray's Anatomy*, Churchill Livingstone, Edinburgh

[9] Ahlstrom, C. (2006a). "Processing for the Phonocardiographic Signal - Methods for the Intelligent Stethoscope," Linköping University, Sweden.

[10] Berne, R. M., and Levy, M. N. (1997). *Cardiovascular Physiology: Mosby's Physiology Monograph Series*, Mosby, St. Louise, Missouri,.

[11] H. Sava and J. McDonnell, "Spectral composition of heart sounds before and after mechanical heart valve implantation using a modified forward-backward prony's method," *Biomedical Engineering, IEEE Transactions on*, vol. 43, no. 7, pp. 734–742, 1996.

[12] H. Sava, P. Grant, and J. McDonnell, "Spectral characterization and classification of carpentier-edwards heart valves implanted in the aortic position," *Biomedical Engineering, IEEE Transactions on*, vol. 43, no. 10, pp. 1046–1048, 1996

[13] S. Aggio, E. Baracca, C. Longhini, C. Brunazzi, L. Longhini, G. Musacci, and C. Fersini, "Noninvasive estimation of the pulmonary systolic pressure from the spectral analysis of the second heart sound," *Acta cardiologica*, vol. 45, no. 3, pp. 199–202, 1990.

Bibliographical references

[14] C. Longhini, E. Baracca, C. Brunazzi, M. Vaccari, L. Longhini, and F. Barbaresi, "A new noninvasive method for estimation of pulmonary arterial pressure in mitral stenosis," *The American journal of cardiology*, vol. 68, no. 4, pp. 398–401, 1991.

[15] Zhang, X. Y., and Zhang, Y. T. "A Novel Method for the Noninvasive and Continuous Monitoring of Arterial Blood Pressure on an Electronic Stethoscope." *3rd European Medical & Biological Engineering Conference.*, Prague, Czech Republic, 4602-4605

[16] H. Koymen, B. Altay, and Y. Ider, "A study of prosthetic heart valve sounds," *Biomedical Engineering, IEEE Transactions on*, no. 11, pp. 853–863, 1987.

[17] A. Oppenheim, R. Schafer, J. Buck, *et al.*, *Discrete-time signal processing*. Prentice hall Upper Saddle River^ eN. JNJ, 1989, vol. 2.

[18] Leatham A: Systolic murmurs. *Circulation* 1958;17:601-611

[19]. Tavel MD: Innocent murmurs, in Leon DF, Shaver JA (eds): Physiologic Principles of Heart Sounds and Murmurs. AHA Monograph no. 46. New York, American Heart Association, 1975, pp 102-106

[20]. Craige E, Millward DK: Diastolic and continuous murmurs. Prog Cardiovasc Dis 1971 ;14:38-56

[21]. Softer A, Feinstein A, Luisada AA, Perloff JK, Rosner S, Sehlant RC, Segal BL: Glossary of cardiologic terms related to physical diagnosis and history. *Am J Cardiol*

[22] Wickerhauser, 1994; Graps, 1995; Burrus et al., 1998; David, 2002 & 40 Oppenheim & Schafer, 2010.

[23] F. Hlawatsch, G. F. Boudreaux-Bartels, "Linear and Quadric Time-Frequency Signal Representations", IEEE SP Magazine, pp.21-67, April 1992.

[24]Adhemar Bultheel, "Wavelets with applications in signal and image processing(2003)", available at http://www.win.tue.nl/morscheh/2DE10/alltxt.pdf(Accessed: 10 August 2011967;20:285-286

[25] Sweldens, W., Wavelets: what next?, Proceedings of the IEEE, vol. 84, No. 4, pp. 680-685, ISSN 0018-9219, 199

[26] A. V. Oppenheim, R. W. Schafer, *Digital signal processing*, Prentice-Hall, 1975.

[27] J O Stromberg, 'A Modified Franklin System and Higher Order Spline Systems on RN

[28]Adhemar Bultheel, "Wavelets with applications in signal and image processing(2003)", available at http://www.win.tue.nl/~morscheh/2DE10/alltxt.pdf(Accessed: 10 August 2011).

[29] Sweldens, W., Wavelets: what next?, Proceedings of the IEEE, vol. 84, No. 4, pp. 680-685, ISSN 0018-9219, 199

[30] I. Daubechies, Ten Lectures on wavelets, Number 61 in CBMS-NSF Series in Applied

Bibliographical references

Mathematics. SIAM, Philadelphia, 1992

[31] P. G. Lemari´e and Y. Meyer, Ondelettes et bases hilbertienes, Rev. Mat. Iberoamericana, 2 :1-18, 1986

[32] A. V. Oppenheim, R. W. Schafer, *Digital signal processing*, Prentice-Hall, 1975.

[33] J O Stromberg, 'A Modified Franklin System and Higher Order Spline Systems on RN as Unconditional Bases for Hardy Spaces', in W Beckner(editor): Proc. of Conf. In Honour of A Zygmund, 475-493, Wadsworth Mathematics Series, 1992

[34] Y Meyer, 'Ondeletts, Ondeletts et Operateurs', Paris: Hermann, 1990

[35] Stephane G. Mallat. A theory for multiresolution signal decomposition: The wavelet representation. IEEE Transactions on Pattern Analysis and Machine Intelligence, 11, no. 7:674–693, 1989.

[36] M.J.T. Smith and T.P. Barnwell. Exact reconstruction for tree-structured subband coders. IEEE Trans Acoust Speech Signal Processing, 34: 434 − 441, 1986.

[37] S. G. Mallat, A theory for multiresolution signal decomposition : the wavelets representation, IEEE Trans. Patt. Anal. Mach. Intelly 11 (7) :974-693, 1989.

[38] Ronald Parr, Lihong Li, Gavin Taylor, Christopher Painter-Wakefield, and Michael L Littman. An analysis of linear models, linear value-function approximation, and feature selection for reinforcement learning. In Proceedings of the 25th International Conference on Machine Learning, pages 752–759. ACM, 2008.

[39] Gerald Kaiser. A friendly guide to wavelets. Springer, 2010.

[40] I. Daubechies. Ten Lectures on Wavelets. SIAM, 1992.

[41] Michael Unser, Akram Aldroubi, and Murray Eden. A family of polynomial spline wavelet transforms. Signal processing, 30(2):141–162, 1993.

[42] Michael A Unser. Ten good reasons for using spline wavelets. In Optical Science, Engineering and Instrumentation, pages 422–431. International Society for Optics and Photonics, 1997.

[43] Charles K Chui and Jian-zhong Wang. On compactly supported spline wavelets and a duality principle. Transactions of the American Mathematical Society, 330(2):903–915, 1992.

[44]. S. Mallat, A Wavelet Tour of Signal Processing (Academic press, London, 1999)

[45]. D.lee fugal, Book of c*onceptual wavelets ,in digital signal processing ,an in-depth practical approach for the non −mathematician*

Bibliographical references

[46] A. Phinyomark, C. Limsakul, and P. Phukpattaranont, "Optimal wavelet functions in wavelet denoising for multifunction myo-electric control," ECTI Transactions on Electrical Engineering, Electronics, and Communications, vol. 8, no. 1, pp. 43–52, 2010.

[47] Donoho, D. L. & Johnstone, I. M. (1994). Ideal Spatial Adaptation by Wavelet Shrinkage. *Biometrika*, Vol.81, No.3, (October 1901), pp. 425-455, ISSN 0006-3444

[48] Phinyomark, A. ; Limsakul, C. & Phukpattaranont, P. (2009f). A Comparative Study of Wavelet Denoising for Multifunction Myoelectric Control. Proceedings of ICCAE

[49] Donoho, D. L. & Johnstone, I. M. (1995). Adapting to Unknown Smoothness via Wavelet Shrinkage. Journal of the American Statistical Association, Vol.90, No.432, (March 1888), pp. 1200-1224, ISSN 0162-1459

[50] Donoho, D. L. (1995). De-noising by Soft-thresholding. IEEE Transactions on Information Theory, Vol.41, No.3, (1955), pp. 613-627, ISSN 0018-9448

[51] Donoho, D. L. (1992). Wavelet Analysis and WVD: A Ten Minute Tour, In: Progress in Wavelet Analysis and Applications, Meyer, Y. & Roques, S., pp. 109–128, Frontières Ed

[52] Zhong, S. & Cherkassky, V. (2000). Image Denoising Using Wavelet Thresholding and Model Selection. Proceedings of ICIP 2000 International Conference on Image Processing, pp. 262-265, ISBN 0-7803-6297-7, Vancouver, BC, Canada, September 10-13, 2000

[53] Song, G. & Zhao, R. (2001). Three Novel Models of Threshold Estimator for Wavelet Coefficients. Proceedings of WAA 2001 2nd International Conference on Wavelet Analysis and Its Applications, pp. 145-150, ISBN 3-540-43034-2, Hong Kong, China, December 18-20, 2001

[54] Zhang, Q. J. & Luo, Z. Z. (2006). Wavelet De-noising of Electromyography. Proceedings of ICMA 2006 IEEE International Conference on Mechatronics and Automation, pp. 1553- 1558, ISBN 1-4244-0465-7, Luoyang, China, June 25-28, 2006

[55] Elena, M. M. ; Quero, J. M. & Borrego, I. (2006). An Optimal Technique for ECG Noise Reduction in Real Time Applications. Proceedings of CinC 2006 Computers in Cardiology, pp. 225-228, ISBN 978-1-4244-2532-7, Valencia, Spain, September 17-20, 2006

[56] Johnstone, I. M. & Silverman, B. W. (1997). Wavelet Threshold Estimators for Data with Correlated Noise. Journal of the Royal Statistical Society: Series B (Statistical Methodology), Vol.59, No.2, (1934), pp. 319-351, ISSN 1369-7412

[57] Percival, D. B. & Walden, A. T. (2000). Wavelet Methods for Time Series Analysis, Cambridge University Press, ISBN 0-521-64068-7, USA

[58] Vidakovic, B. (1999). Statistical Modeling by Wavelets, John Wiley & Sons, ISBN 978-0-471- 29365-1, USA

[59] Guo, X.; Yang, P.; Li, L. F. & Yan, W. L. (2004b) Study and Analysis of Surface EMG for the Lower Limb Prosthesis. Proceedings of ICMLC 2004 3rd International Conference on Machine Learning and Cybernetics, pp. 3736-3740, ISBN 0-7803-8403-2, Shanghai, China, August 26-29, 2004

[60] Poornachandra, S.; Kumaravel, N.; Saravanan, T. K. & Somaskandan, R. (2005). WaveShrink Using Modified Hyper-shrinkage Function. Proceedings of IEEE-EMBS 2005 27th Annual International Conference of the Engineering in Medicine and Biology Society, pp. 30-32, ISBN 0-7803-8741-4, Shanghai, China, January 17-18, 2006

[61] Gao, H. Y. (1998). Wavelet Shrinkage Denoising Using the Non-negative Garrote. Journal of Computational and Graphical Statistics, Vol.7, No.4, (1992), pp. 469-488, ISSN 1061- 8600

[61] Guo, X. ; Yang, P. ; Li, Y. & Yan, W. L. (2004a) The SEMG Analysis for the Lower Limb Prosthesis Using Wavelet Transform. Proceedings of IEMBS 2004 26th Annual

[62] Guo, X.; Yang, P.; Li, L. F. & Yan, W. L. (2004b) Study and Analysis of Surface EMG for the Lower Limb Prosthesis. Proceedings of ICMLC 2004 3rd International Conference on Machine Learning and Cybernetics, pp. 3736-3740, ISBN 0-7803-8403-2, Shanghai, China, August 26-29, 2004

[63] Tianshu, Q.; Shuxun, W.; Haihua, C. & Yisong, D. (2002). Adaptive Denoising based on Wavelet Thresholding Method. Proceedings of ICOSP 2002 6th International Conference on Signal Processing, pp. 120-123, ISBN 0-7803-7488-6, Beijing, China, August 26-30, 2002

[64] Su, L. & Zhao, G. (2005). De-noising of ECG Signal Using Translation-invariant Wavelet Denoising Method with Improved Thresholding. Proceedings of IEEE-EMBS 2005 27th Annual International Conference of the Engineering in Medicine and Biology Society, pp. 5946-5949, ISBN 0-7803-8741-4, Shanghai, China, January 17-18, 2006

[65] Lehmann, E. L.; Casella, George (1998). Theory of Point Estimation (2nd ed.). New York: Springer. ISBN 0-387-98502-6. MR 1639875.

[66] Bushberg, J. T., et al., *The Essential Physics of Medical Imaging*, (2e). Philadelphia: Lippincott Williams & Wilkins, 2006, p. 280.

[67] Guohualu "Removing ECG noise from surface EMG signals using adaptive filtering" journal Elsevier Ireland Ltd 462(2009), pp. 14-19

[68] www. egeneralmedical.com/listohearmur.html

[69] Bentley, P., Nordehn, G., Coimbra, M., Mannor, S. 2011.The PASCAL Classifying Heart Sounds Challenge 2011.www.peterjbentley.com/heart challenge/index.html.

[70] Xiefeng Cheng and Zheng Zhang 'Denoising method of heart sound signals based on self-construct heart sound wavelet'AIP ADVANCES 4, 087108 (2014)

[71]. Tahar Omari, An automatic wavelet denoising scheme for heart sounds .International Journal of Wavelets, Multiresolution and Information Processing. Vol.13, No. 3 (2015) 1550016 (21 pages). DOI: 10.1142/S0219691315500162

[72]. M. Abhishek, G.R. Sinha, Denoising of PCG signal by using wavelet transforms. Adv. Comput. Res.4 (1), 46–49 (2012)

[73]. M. Abhishek et al., Comparison of wavelet transforms for denoising and analysis of PCG signal. IManag. J. Commun. Eng. Syst. 1(1), 48–52 (2011)

[74]. G. Dawid, G. Redlarski, Wavelet-based denoising method for real phonocardiography signal recorded by mobile devices in noisy environment. Comput. Biol. Med. 52, 119–129 (2014)

[75]. Mohammed Nabih Ali• EL-Sayed A. El-Dahshan 'Denoising of Heart Sound Signals Using Discrete Wavelet Transform. Circuits Syst Signal Process. (2017) 36:4482–4497 DOI 10.1007/s00034-017-0524-7

[76]. Abhishek Misal, G. R. Sinha, 'Separation of Lung Sound from PCG Signals Using Wavelet Transform', Journal of Basic and Applied Physics, Aug. 2012, Vol. 1 Iss. 2, PP. 57-61

[77] Gopi Bhanushali and Narendra B, 'ECG Signal De-noising using Discrete Wavelet Transform for Removal of
AWGN Noise by Daubenchies Technique', JSRD - International Journal for Scientific Research & Development| Vol. 2, Issue 01, 2014 | ISSN (online): 2321-0613

 [78]. L. Feng, Y. Wang, Y. Wang, Research and implementation of heart sound denoising. Phys. Procedia 25, 777–785 (2012)